

See discussions, stats, and author profiles for this publication at: <https://www.researchgate.net/publication/226165534>

NiTi and NiTi–TiC composites: Part IV. Neutron diffraction study of twinning and shape-memory recovery

Article in *Metallurgical and Materials Transactions A* · September 1996

DOI: 10.1007/BF02652374

CITATIONS

67

READS

95

4 authors, including:



David C Dunand

Northwestern University

425 PUBLICATIONS 10,441 CITATIONS

[SEE PROFILE](#)



Daniele Mari

École Polytechnique Fédérale de Lausanne

100 PUBLICATIONS 1,434 CITATIONS

[SEE PROFILE](#)



Mark Bourke

Los Alamos National Laboratory

191 PUBLICATIONS 3,740 CITATIONS

[SEE PROFILE](#)

Some of the authors of this publication are also working on these related projects:



Cobalt based superalloys by Powder Metallurgy route [View project](#)



Metallic Architectures from 3D-Printed Powder-Based Liquid Inks [View project](#)

NiTi and NiTi-TiC Composites: Part IV. Neutron Diffraction Study of Twinning and Shape-Memory Recovery

D.C. DUNAND, D. MARI, M.A.M. BOURKE, and J.A. ROBERTS

Neutron diffraction measurements of internal elastic strains and crystallographic orientation were performed during compressive deformation of martensitic NiTi containing 0 vol pct and 20 vol pct TiC particles. For bulk NiTi, some twinning takes place upon initial loading below the apparent yield stress, resulting in a low apparent Young's modulus; for reinforced NiTi, the elastic mismatch from the stiff particles enhances this effect. However, elastic load transfer between matrix and reinforcement takes place above and below the composite apparent yield stress, in good agreement with continuum mechanics predictions. Macroscopic plastic deformation occurs by matrix twinning, whereby (1 0 0) planes tend to align perpendicular to the stress axis. The elastic TiC particles do not alter the overall twinning behavior, indicating that the mismatch stresses associated with NiTi plastic deformation are fully relaxed by localized twinning at the interface between the matrix and the reinforcement. For both bulk and reinforced NiTi, partial reverse twinning takes place upon unloading, as indicated by a Bauschinger effect followed by rubberlike behavior, resulting in very low residual stresses in the unloaded condition. Shape-memory heat treatment leads to further recovery of the preferred orientation and very low residual stresses, as a result of self-accommodation during the phase transformations. It is concluded that, except for elastic load transfer, the thermal, transformation, and plastic mismatches resulting from the TiC particles are efficiently canceled by matrix twinning, in contrast to metal matrix composites deforming by slip.

I. INTRODUCTION

THE shape-memory effect exhibited by near-stoichiometric NiTi-based alloys originates from the thermoelastic phase transformation between an ordered, high-temperature phase B2 (austenite) and an ordered, low-temperature phase B19' (martensite) deforming by twinning. The conclusions of several recent reviews^[1-8] are summarized in the following. Upon transformation from austenite to martensite in the absence of external or internal stresses, the martensite microstructure consists of equal proportions of the 24 crystallographically possible martensitic variants with different orientations, as a result of self-accommodation reducing the internal transformation strains. Upon mechanical loading, variant conversion takes place, such that the variant resulting in the largest strain in the direction of the applied stress grows at the expense of the other, less favorably oriented variants. The conversion between variants, which is equivalent to a twinning operation, results in a macroscopic strain and a preferred orientation of the martensite. While, in some cases, partial reverse twinning is observed upon mechanical unloading (rubberlike behavior), the twinning strain is usually conserved upon removal of the external stress. Upon subsequent transformation of the twinned martensite, austenite is formed with the same orientation as that prior to deformation, because a unique lattice correspondence exists between the two ordered phases and because

the transformation is crystallographically reversible. Therefore, the macroscopic twinning strain developed in the deformed martensite phase is recovered and the specimen reverts to its previous, undeformed shape (shape-memory effect). If, upon subsequent cooling, the martensitic variants formed during the transformation are again randomly oriented, the strain recovery is conserved (one-way shape-memory effect). However, if the previously oriented martensite variants are formed as a result of biasing by internal stresses, the macroscopic strain recovery is partially or fully canceled (two-way shape-memory effect).

Because the NiTi phase transformation is thermoelastic, it is very sensitive to external or internal stresses. Internal mismatch stresses produced by the reinforcing second phase in NiTi-based metal matrix composites may thus affect both the matrix transformation behavior (*e.g.*, hysteresis, thermal cycling, shape-memory recovery, and stress-induced martensite formation) and its deformation behavior (twinning, rubberlike effect and pseudoelastic deformation). In part I of this article series,^[9] we examined in NiTi-TiC composites the effect of elastic, nontransforming TiC particles upon the thermally-induced phase transformation behavior of the undeformed NiTi matrix and found that the internal mismatch stresses indeed alter the thermodynamics and kinetics of the thermoelastic transformation. In parts II^[10] and III,^[11] we reported on a systematic investigation of the mechanical deformation and shape-memory effect of these composites. In the present article, we use neutron diffraction to study the internal strains and preferred orientation of unreinforced NiTi and NiTi containing 20 vol pct TiC particles. We examine these materials during mechanical loading where twinning is the main deformation mechanism, during mechanical unloading where reverse twinning takes place, and before and after shape-memory recovery by phase transformation. We discuss our results in light of

D.C. DUNAND, AMAX Associate Professor, is with the Department of Materials Science and Engineering, Massachusetts Institute of Technology, Cambridge, MA 02139. D. MARI, CEO, is with Advanced Composite and Microwave Engineering, 1015 Lausanne, Switzerland. M.A.M. BOURKE, Technical Staff Member, MST5, and J.A. ROBERTS, Acting Center Leader, LANSCE, are with the Los Alamos National Laboratory, Los Alamos, NM 87545.

Manuscript submitted January 23, 1995.

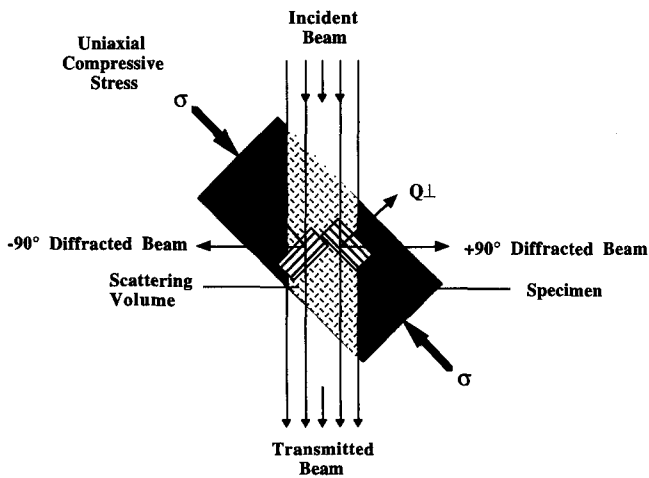


Fig. 1—Schematic configuration of neutron diffraction experiment with scattering vector definitions. Diffraction of planes parallel to the applied stress gives strains perpendicular to the stress axis and is detected at an angle of +90 deg with the incident beam. Respectively, diffraction of planes perpendicular to the applied stress gives strains parallel to the stress axis and is detected at an angle of -90 deg with the incident beam.

thermal, allotropic, elastic, and plastic mismatches between the NiTi matrix and the TiC reinforcement, as well as of matrix preferred orientation by twinning. To the best of our knowledge, this article series is the first report of the mechanical behavior of a discontinuously reinforced metal matrix composite, the main deformation mechanism of which is twinning, as well as of the effect of a second phase upon the shape-memory effect of NiTi.

II. EXPERIMENTAL PROCEDURES

A. Sample Fabrication

Prealloyed NiTi powders (99.9 pct pure, 70- μm average size, from Special Metals Corp., New Hartford, NY) were blended with 20 vol pct equiaxed TiC powders (99.5 pct pure, with size between 44 and 100 μm , from Cerac, Inc., Milwaukee, WI). The powder mixture was poured in a graphite die lined with titanium foil coated with boron-nitride to avoid carbon contamination, and it was vacuum hot pressed for 5.25 to 5.5 hours under a pressure of 22 to 27 MPa at a temperature of 1080 °C. The densified specimen was then subjected to containerless hot isostatic pressing for 2 hours under an argon pressure of 172 MPa (99.999 pct pure) at a temperature of 1160 °C. Furthermore, an unreinforced NiTi specimen was fabricated following the same processing route. As reported in part I,^[9] the matrix is titanium rich (51.4 at. pct Ti) and martensitic at room temperature. Accordingly, the transformation temperatures (measured by differential scanning calorimetry at a scanning rate of 20 K·min⁻¹) are all above room temperature: $A_s = 94$ °C and $A_f = 119$ °C upon heating; $M_s = 70$ °C and $M_f = 55$ °C upon cooling for bulk NiTi; and $A_s = 82$ °C, $A_f = 117$ °C, $M_s = 70$ °C, and $M_f = 47$ °C for the composite.^[9,12]

Two cylindrical compression samples (9.9 mm in diameter and 24 mm in length) were fabricated by electrodischarge machining from the center portion of the unreinforced and reinforced specimens, respectively, re-

ferred to in the following as NiTi and NiTi-20TiC. To minimize residual stresses and anneal the matrix, the machined samples were kept for 1 hour at 930 °C under titanium-gettered, flowing argon and subsequently furnace cooled to 400 °C and air cooled to room temperature. As reported in part I,^[9] no reaction or dissolution of TiC occurred during the heat treatments.

B. Neutron Scattering Measurements

Because diffraction techniques are phase specific and sensitive to crystal structure, crystal orientation, and lattice strains, they are well suited to study composite materials with multiple phases exhibiting different residual or applied strains, as well as shape-memory alloys exhibiting twinning and phase transformations. While either X-rays or neutrons can be used, the two types of radiation differ in the volume of material sampled during measurement.^[13,14,15] For the soft wavelengths (1 to 3 Å) suitable for crystalline diffraction, X-ray penetration depths are typically several orders of magnitude less than for thermal neutrons in most materials. For NiTi, the 50 pct transmission thickness for Cu K_α X-rays is approximately 9 μm , compared to about 3 cm for thermal neutrons.^[16] The bulk measurements possible with neutron diffraction are particularly important for our specimens, because the reinforcement is coarse (about 70 μm) and because the matrix is thermoelastic and thus sensitive to stress relaxation at free surfaces.

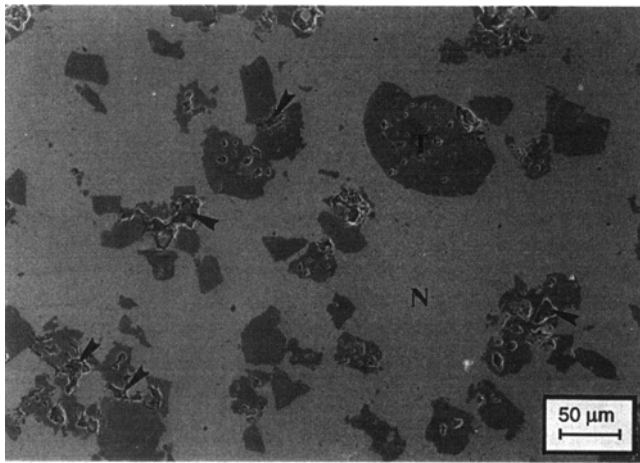
Neutron diffraction measurements were performed in “time of flight” mode using the neutron powder diffractometer at the pulsed neutron source at the Manuel Lujan Jr. Neutron Scattering Center (Los Alamos National Laboratory, Los Alamos, NM). Because each pulse of neutrons contains a continuous wavelength spectrum, a detector at a fixed angle collects a complete diffraction pattern for each pulse. The reflection lattice spacings d_{hkl} are determined through Bragg’s relationship, and the elastic strain, ϵ , for a set of hkl planes is calculated from

$$\epsilon = \frac{(d_{hkl} - d_0)}{d_0} = \frac{\Delta d}{d_{hkl}} \quad [1]$$

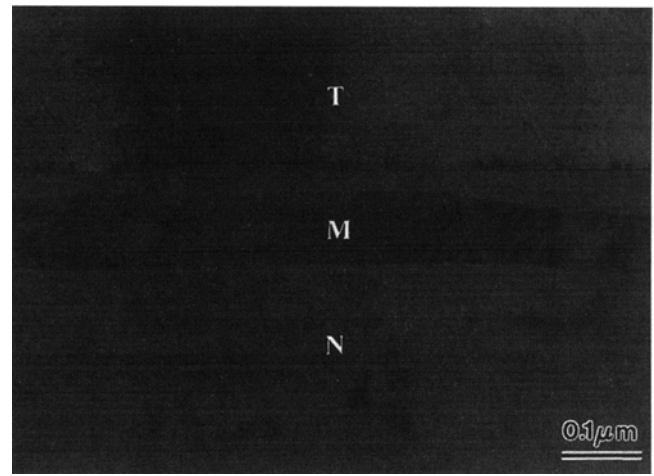
where d_0 is the reference plane spacing and Δd is the shift in plane spacing.

The NiTi and NiTi-20TiC compression samples were deformed in a modified mechanical tester, described in References 17 and 18, with a loading axis forming an angle of 45 deg with the incident neutron beam. Strains parallel and perpendicular to the loading axis were measured simultaneously by two detectors forming an angle with respect to the incident beam of -90 deg (Q parallel to the load) and +90 deg (Q perpendicular to the load), respectively (Figure 1). Because the detectors subtend a finite angle $2\theta = 11$ deg, strains are averaged over an angle $\theta = 5.5$ deg; this small error is neglected in the following discussion. Since the sample is scanned in wavelength, the fixed detectors collect all possible Bragg reflections with the same scattering vector Q . The diffraction volume was 1.1 cm³, comprising 60 pct of the total specimen volume.

Bragg reflections with lattice spacings between 0.5 to about 4 Å were recorded by the two detectors, and each spectrum was divided by the total incident fluence. The program FITPEAKS^[19] was used to fit to individual Bragg



(a)



(b)

Fig. 2—(a) Scanning electron micrograph of NiTi-20TiC showing somewhat porous TiC particles (T) in the NiTi matrix (N). Some particles are clustered resulting in matrix porosity (arrows). (b) Transmission electron micrograph of NiTi-20TiC showing part of a platelike TiC particle (T) within the NiTi matrix (N) with a martensitic plate (M) parallel to the TiC particle.

reflections with an asymmetric peak shape characteristic of the diffractometer. The fits give both the peak centers, from which elastic strains are calculated with Eq. [1], and the integrated peak intensities, which are proportional to the number of grains in the diffracting condition. Changes in the intensities of individual reflections quantify the fraction of NiTi variants in the diffraction condition. To describe these changes, we define a normalized scale factor as the ratio of a peak intensity to its intensity under zero load.

The average material response was determined using the Rietveld approach^[20] using the Los Alamos generalized structure analysis system (GSAS) program,^[21] whereby the intensities and positions of all Bragg peaks are predicted from an assumed crystal structure. Strains are calculated using Eq. [1] with lattice parameters determined by least-squares fits between observed and predicted spectra. Due to ambiguities associated with using the powders as stress-free samples, the unstressed, annealed bulk samples were used as a stress-free reference. The contributions of thermal and transformation mismatch strains in these reference samples are estimated later.

Two strain gages with 3-mm gage length were attached on diametrical sides of the samples to record the macroscopic strain, which includes both elastic and plastic components. The first diffraction measurement was performed at a small applied compressive stress of -3 MPa, required to hold the specimen in position. The nominal stress was then increased at a strain rate of about 10^{-3} s^{-1} to -100 MPa (-90 MPa for the NiTi sample), -210 MPa, and -280 MPa, followed by a decrease to -100 MPa and -3 MPa. The specimens were held under load control while diffraction data were collected for 4 hours for NiTi and 5 hours for NiTi-20TiC. At some stress levels, the hold time was longer due to interruptions of the neutron beam. Both samples exhibited small amounts of relaxation after each stress change, but since relaxation was relatively small and the stress was maintained constant, relaxation is not considered to affect the diffraction measurements.

On completion of the mechanical loading cycle, the samples were removed from the mechanical tester and recovered above A_f in an oil bath held between 150 °C and 175

°C for a total time of 5 minutes for NiTi and 12 minutes for NiTi-20TiC. After cooling to room temperature, each sample was replaced in the mechanical tester and the diffraction patterns measured at a nominal stress of -3 MPa. The sample lengths were measured using a micrometer before and after loading, as well as after recovery.

III. RESULTS

The density of as-fabricated NiTi samples was measured by water displacement as $6.42 \text{ g}\cdot\text{cm}^{-3}$, *i.e.*, 99.5 pct of the theoretical density of $6.45 \text{ g}\cdot\text{cm}^{-3}$.^[22] The density of the NiTi-20TiC samples was $5.62 \text{ g}\cdot\text{cm}^{-3}$ for the control sample and $5.59 \text{ g}\cdot\text{cm}^{-3}$ for the sample used for diffraction measurements. These values are, respectively, 91.4 and 91.0 pct, of the theoretical composite density, calculated from the rule of mixture with a TiC density of $4.93 \text{ g}\cdot\text{cm}^{-3}$.^[23] As shown in Figure 2(a), TiC particles are somewhat porous and tend to form clusters, with which matrix porosity is often associated. While particle internal porosity is not expected to significantly affect the matrix stress state, matrix porosity may influence the mechanical behavior of the materials by altering locally the matrix stress field or by reducing mismatch between the particle and matrix. Except for the correction of the effective cross-sectional area described in the following paragraph, however, we neglect the effect of porosity upon the mechanical properties of the matrix. Figures 2(a) and (b) furthermore demonstrate that the TiC interface is unreacted and well bonded with the matrix and that no TiC dissolution and reprecipitation took place during processing. Finally, Figure 2(b) shows a martensitic plate oriented parallel to the TiC particle main axis, illustrating the effect of the residual stress field upon plate orientation.

Figure 3 shows the superimposed stress-strain plots of NiTi and NiTi-20TiC. The strain values are an average of the two strain-gage measurements which showed negligible differences, as expected if buckling is absent. To take into account porosity, the stress values are corrected by multiplying the cross-sectional area of the samples by their rel-

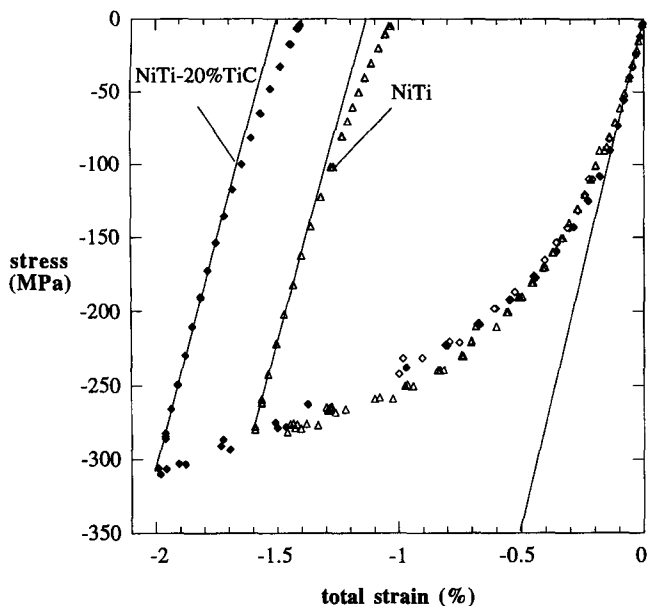


Fig. 3—Stress-strain curves of the NiTi sample (triangles) and the two NiTi-20TiC samples (open lozenges: sample used for neutron experiment; filled lozenges: sample tested outside neutron beam, without hold periods). Strain is measured by strain gages.

ative density. Because the same nominal (density-uncorrected) maximum stress was used for all samples (−280 MPa), the corrected maximum stress for NiTi-20TiC was higher than for NiTi. Two experiments were performed for NiTi-20TiC. First, the macroscopic strain of the specimen used for neutron measurement was measured by strain gage up to a nominal stress of −220 MPa only. Second, the control specimen was mechanically tested according to the same stress history as the previous sample but without diffraction measurements and the associated holding periods. As shown in Figure 3, the stress-strain plots of the two NiTi-20TiC specimens superimpose closely, indicating that the strain-gage measurements were reproducible. Table I summarizes the mechanical properties derived from the stress-strain curves of NiTi and NiTi-20TiC (Figure 3).

The Rietveld procedure on the unloaded NiTi diffraction spectrum gives the best fit with the $P112_1/m$ structure, confirming the generally admitted structure.^[24,25] No match with the $P2/c$ structure was found, in contrast to the neutron diffraction measurements in Reference 26. Crystallographic data of undeformed samples are given in Table II, with b as the unique axis of the monoclinic cell, a convention used in the remainder of this article.

Figure 4(a) shows for NiTi the lattice strain ϵ_{ijk} for plane (ijk) , calculated from Eq. [1], as a function of the applied stress σ_A upon mechanical loading. While deviations from the elastic line seem to occur at high stresses for the elastic gradients, σ_A/ϵ_{ijk} , we cannot assign these deviations to a physical phenomenon, such as load transfer between variants as a result of twinning, because the best-fit lines connect the error bars of almost all data points. In contrast, Figure 4(b) for NiTi-20TiC exhibits both higher elastic gradients and significant deviations for the elastic lines at high stresses, indicating that load transfer is taking place between the matrix and the particles.

Figures 5(a) and (b) show the scale factor ratios of the most intense, overlap-free Bragg reflections as a function

of the plastic strain during loading, defined as the macroscopic strain-gage measurement less the elastic strain calculated from the macroscopic Young's modulus. Because the scale factor ratios are proportional to the integrated peak intensities, they are a good measure of the volume fraction of variants with planes in the Bragg condition and thus of preferred orientation. The systematic increase or decrease of the scale factor ratios indicates that a texture develops upon deformation as a result of twinning. The composite exhibits the same preferred orientation behavior as the bulk matrix (Figures 5(a) and (b)), and the rate of change of the scale factor ratios as a function of the plastic strain is generally similar for both, indicating that the TiC particles have only a small effect on the average twinning behavior of the matrix.

Upon unloading, the scale factor ratios of NiTi and NiTi-20TiC evolve quite differently, as depicted in Figures 6(a) and (b) and 7(a) and (b). Furthermore, in contrast to loading (Figures 5(a) and (b)), there is upon unloading no linear relationship between scale factor ratios and plastic strain: in many cases, the scale factor ratio/plastic strain curves exhibit a change of slope sign, indicative of a complex twinning behavior. In most cases, a trend to reversion toward the undeformed state, however, is observed for the scale factor ratios upon shape-memory recovery but not in the reversible fashion suggested by the dotted line in Figures 6(a) and (b) and 7(a) and (b).

Figures 8 and 9 show for NiTi and NiTi-20TiC, respectively, the residual strains for the most important planes, under zero applied stress after mechanical unloading and after shape-memory recovery. While the sign of the residual strains varies between these two states, their magnitude and average are similar, indicating that mismatch relaxation has taken place. Comparison of Figures 8 and 9 also shows that residual strains for all measured planes are similar for NiTi and NiTi-20TiC. Also shown in these figures is the average residual strain after unloading and recovery, calculated as the mean of the residual strains in the three cell directions determined from the crystallographic constants in Table II.

IV. DISCUSSION

The macroscopic stress-strain plots displayed in Figure 3 and the mechanical properties listed in Table I show that NiTi and NiTi-20TiC behave macroscopically in a very similar manner. First, the Young's modulus and the yield stress (taken as the proportional limit, *i.e.*, the first measurable deviation from the elastic line in Figure 3) are, within experimental errors, the same for the composite and the bulk material upon both mechanical loading and unloading. Second, for both samples, the unloading portion of the stress-strain plot is curved, resulting in a strain recovery larger than expected from the extrapolation of the linear portion of the unloading trace. This nonlinear recovery (rubberlike behavior) is similar for both materials. Finally, while the shape-memory recovery strain is higher for the composite, the recovery strain normalized by the plastic strain after mechanical unloading is, within experimental errors, similar for both samples. A systematic study of the shape-memory effect in NiTi-TiC composites is presented in part III of this article series.^[11]

The close overlap of stress-strain plots for NiTi and

Table I. Mechanical Properties of NiTi and NiTi-20TiC Deformed in Compression

	NiTi	NiTi-20TiC	Estimated Error
Elastic modulus (loading) (GPa)	69	71	± 4
(unloading)	61	64	± 4
Yield stress (loading) (MPa)	-40	-50	± 5
(unloading)	-160	-150	± 5
Rubberlike strain recovery upon unloading (pct)	-0.10*	-0.11*	± 0.02
Permanent strain after unloading (pct)	-1.04*	-1.41*	± 0.02
	-1.08**	-1.47**	± 0.02
Strain recovered by shape memory (pct)	-0.83**	-1.07**	± 0.02
Fraction of permanent strain recovered by shape memory (pct)	77	73	± 3

*Strain-gage measurement.
**Micrometer measurement.

NiTi-20TiC (Figure 3) is unexpected, since elastic, perfectly plastic composites containing equiaxed particles exhibit a Young's modulus, yield strength, and strain-hardening rate that are significantly higher than for their unreinforced matrix.^[27,28,29] However, for NiTi, the main plastic deformation mechanism is by twinning of the martensite variants, while for a non-twinning metal, plastic deformation is produced by slip through dislocation motion. This important difference is discussed in the remainder of this section in light of the neutron diffraction results upon mechanical loading, mechanical unloading, and thermal recovery. Furthermore, the stress-strain behavior at higher strains, for which the mechanical behaviors of reinforced and unreinforced NiTi are different, is discussed in part II of this article series.^[10]

A. Elastic Deformation upon Mechanical Loading

1. NiTi

Using both individual peaks and lattice parameters determined by the Rietveld method, strain determination between the undeformed bulk NiTi sample and the NiTi powders proved to be inconclusive (Table II). The main problem associated with the use of powder samples as references for absolute strain calculations is the difference in scattering geometry between powders contained in vanadium cans and bulk samples located in the mechanical tester, which can induce time-of-flight errors. Also, small variations in the NiTi crystallographic parameters may have resulted from the consolidation step, during which the NiTi composition may have varied slightly, as a result of reaction with adsorbed oxygen. Finally, the state of microstress for self-accommodating martensitic variants in a rapidly solidified powder with a large surface-to-volume ratio may significantly differ from that of constrained variants in the bulk after consolidation and heat treatment. Therefore, we have used in the following the undeformed state of the respective samples as the reference state. If the assumption that there are no initial residual stresses is correct, then the calculated strains are absolute; otherwise, the strain measurements are relative to the initial state of the material. Because the NiTi thermoelastic transformation near room temperature is self-accommodating, internal strains and stresses are expected

to be minimized, and the reported strain values are expected to be close to their absolute values.

The elastic modulus for a given crystal direction, $E_{hkl} = \sigma_{hkl}/\epsilon_{hkl}$, does not usually correspond to the measured elastic gradient σ_A/ϵ_{hkl} (Figure 4), because the internal stress σ_{hkl} and the externally applied stress σ_A can differ as a result of the anisotropy of elastic constants. The Hill average, which is the average between the isostress Reuss limit (where σ_{hkl} and σ_A are equal) and the isostrain Voigt limit, gives the best agreement with diffraction data of many materials.^[13] The calculation of the Young's modulus for NiTi from the measured elastic gradients (Figure 4(a)), however, is difficult, because the stress on single martensitic variants is ill defined as a result of load transfer and compatibility mismatch between variants. Furthermore, 12 independent elastic constants are needed to describe monoclinic NiTi. As described in Appendix A, by assuming a cubic symmetry and using the measured elastic gradient of (1 0 0) planes and two other elastic constants determined by Brill *et al.*,^[30] we calculate an average Young's modulus $\bar{E} = 76$ GPa. In view of experimental errors and the preceding simplifying assumptions, this value is in reasonable agreement with the macroscopic modulus measured by strain gages ($E = 69 \pm 4$ GPa upon loading, Table I), the modulus measured by internal friction for stoichiometric NiTi ($E = 68$ to 70 GPa),^[31] and the mean of the Voigt and Reuss averages assuming a cubic structure^[13] ($E = 69$ GPa), calculated from single-crystal ultrasonic measurements^[30] for Ni-49.5 at. pct Ti at 250 K (corresponding to the same undercooling below M_s as our samples).

The small difference found between the calculated and measured moduli may be the result of small amounts of twinning in the apparently linear region of the stress-strain curve, as further discussed in Section 2. This hypothesis is strengthened by the observation by Bührer *et al.*^[32] that variant reorientation takes place upon application of a small tensile stress of 56 MPa in a drawn NiTi wire. Direct observation by neutron diffraction indicated that the intensity of some diffraction peaks was strengthened at the expense of others; a further indirect confirmation of twinning was given by the decrease of internal friction under stress, indicating a lower density of interface, resulting from variant reorientation.^[32]

2. NiTi-TiC

As for most metal matrix composite systems cooled from an elevated processing temperature, NiTi-20TiC is expected to exhibit residual thermal mismatch stresses due to the difference in coefficients of thermal expansion between reinforcement and matrix.^[33,34] Furthermore, additional mismatch stresses between the two phases of the NiTi-20TiC specimens are expected due to the volume and shape changes upon the allotropic transformation of NiTi. These thermal and allotropic mismatch contributions are calculated in Appendix B by the Eshelby method. Table III lists the mean internal stress and strain at room temperature for both phases of the composite, as calculated from Eqs. [B1] through [B8] and the following coefficients of thermal expansion: $\alpha_i = 7.3 \cdot 10^{-6} \text{ K}^{-1}$ for TiC between 25 °C and 750 °C,^[23] $\alpha_m = 11 \cdot 10^{-6} \text{ K}^{-1}$ for austenitic NiTi between M_s and 750 °C,^[22] and $\alpha_m' = 8.5 \cdot 10^{-6} \text{ K}^{-1}$ for martensitic NiTi between room temperature and A_s .^[11] The expansion of the matrix upon allotropic transformation $\epsilon_{A-M}^* = -7.8 \cdot 10^{-4}$, as

Table II. Crystallographic Data from Rietveld Refinement of Spectra Gathered on the -90 Deg Detector

Sample	Temperature (°C)	NiTi				TiC a (Å)
		a (Å)	b (Å)	c (Å)	γ (Deg)	
NiTi (powder)	25	2.9035 ± 3 · 10 ⁻⁴	4.6563 ± 4 · 10 ⁻⁴	4.1167 ± 3 · 10 ⁻⁴	97.66 ± 9 · 10 ⁻³	—
TiC (powder)	25	—	—	—	—	4.3258 ± 1 · 10 ⁻⁴
NiTi (undeformed)	24	2.9039 ± 2 · 10 ⁻⁴	4.6612 ± 3 · 10 ⁻⁴	4.1178 ± 2 · 10 ⁻⁴	97.740 ± 6 · 10 ⁻³	—
NiTi-TiC (undeformed)	31	2.9025 ± 2 · 10 ⁻⁴	4.6560 ± 4 · 10 ⁻⁴	4.1220 ± 3 · 10 ⁻⁴	97.61 ± 9 · 10 ⁻³	4.3299 ± 2 · 10 ⁻⁴

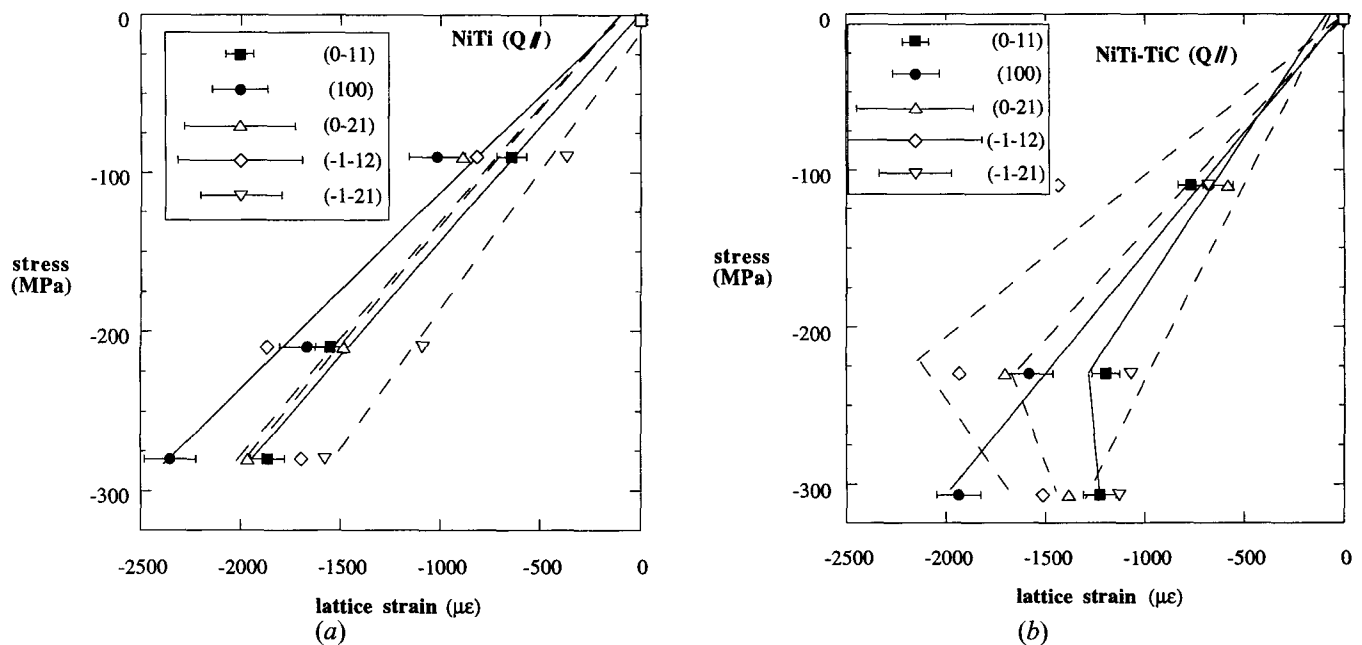


Fig. 4—NiTi lattice strains as a function of applied stress upon compression loading for planes perpendicular to the applied stress (-90 deg). Error bars are shown for the data points of planes (0 -1 1) and (1 0 0) connected by full lines. Typical error bars are given in the legend for the other planes, the data points of which are connected with dotted lines: (a) for bulk NiTi (lines are linear regression fits); and (b) for reinforced NiTi-20TiC.

measured by dilatometry in part III,^[11] results in room-temperature residual strains smaller by about 30 pct than if no transformation had taken place (Table III). We thus conclude that the residual strains are virtually the same in the undeformed NiTi and the undeformed NiTi-20TiC, since the value of the average matrix strain due to phase mismatch in the composite ($\epsilon = 1.28 \cdot 10^{-4}$, Table III) is on the order of the diffraction measurement accuracy.

As for the NiTi sample, comparisons between the undeformed bulk NiTi-20TiC sample and NiTi-TiC powders mixed in the appropriate ratios were inconclusive; the same sources of error identified in section 1 for NiTi apply to NiTi-20TiC. As for the NiTi samples, we thus assume in the following that the annealed, unloaded NiTi-20TiC sample is strain free and we use this sample as a reference for the deformed samples. As shown in Figure 3, the apparent Young's modulus measured from the macroscopic stress-strain plot for NiTi-20TiC ($E = 71 \pm 4$ GPa, Table I) is similar to that of unreinforced NiTi ($E = 69 \pm 4$ GPa, Table I). However, using the elastic constants for TiC from Reference 35, with the apparent NiTi modulus upon loading reported in Table I and $\nu_{\text{NiTi}} = 0.35$ ^[30] under a cubic assumption, the Young's modulus predicted for the composite

from Eqs. [B13] and [B14] is significantly higher ($E = 95$ GPa). This discrepancy can be explained if the strain gage measurement in the apparently linear region below the macroscopic proportional limit is in fact the sum of an elastic contribution and a twinning contribution. Only a small twinning strain ϵ_t is needed to decrease the modulus from a value $E = 95$ GPa to an apparent macroscopic average $E_{\text{app}} = 71$ GPa:

$$\epsilon_t = \sigma(E_{\text{app}}^{-1} - E^{-1}) \quad [2]$$

For an applied stress $\sigma = -50$ MPa, corresponding to the apparent macroscopic yield stress (Table I), Eq. [2] yields $\epsilon_t = -0.02$ pct. Early twinning in NiTi-20TiC is similar to the continuous yielding behavior observed in metal matrix composites deforming by slip.^[36] Upon application of a small external stress, the yield stress is reached internally as a result of the elastic mismatch between the two phases, resulting in a plastic zone around the particulates. Upon overlap of these plastic zones, the composite yields at an applied stress much lower than the yield stress of the unreinforced matrix, and it may exhibit little or no measurable elastic deformation. Localized matrix twinning, relaxing mismatch strains developed around the stiff TiC particles,

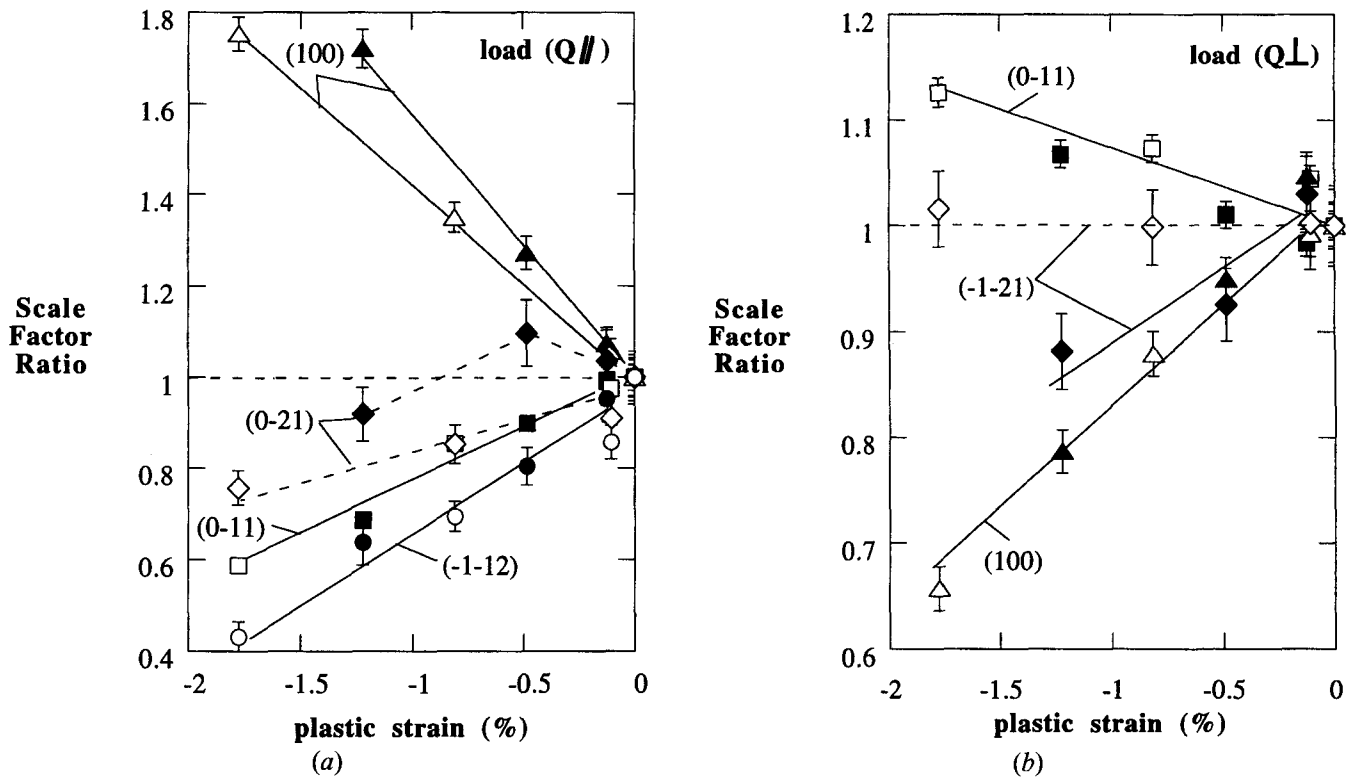


Fig. 5—Normalized scale factor upon mechanical loading as a function of plastic strain for NiTi (filled symbols) and NiTi-20TiC (empty symbols). (a) Planes perpendicular to the applied stress (-90 deg). Plane $(-1 -2 1)$ is not shown, because it does not deviate significantly from a ratio of one. (b) Planes parallel to the applied stress ($+90$ deg). Plane $(0 -2 1)$ is not shown, as it does not exhibit a significant trend; plane $(-1 -1 2)$ is not shown, as its Bragg peak overlapped with other peaks.

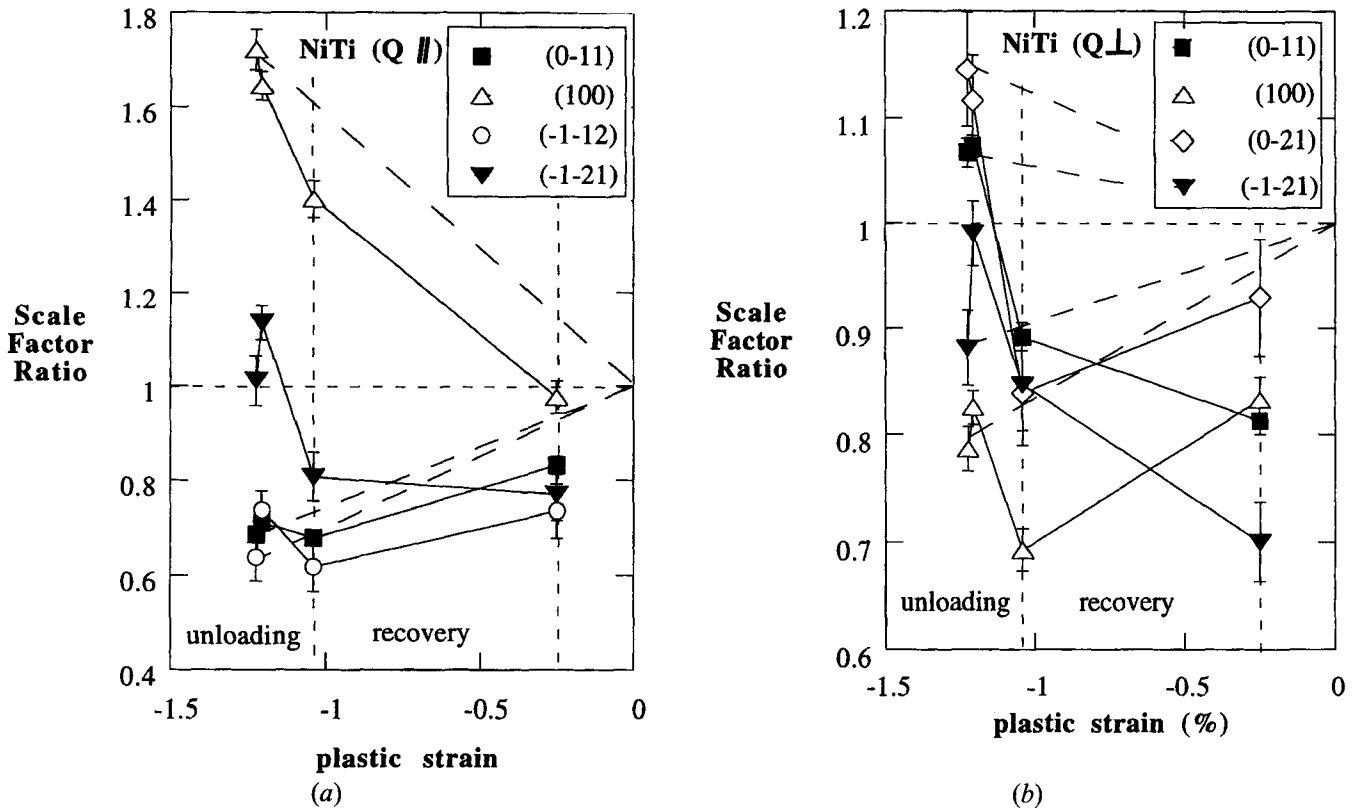
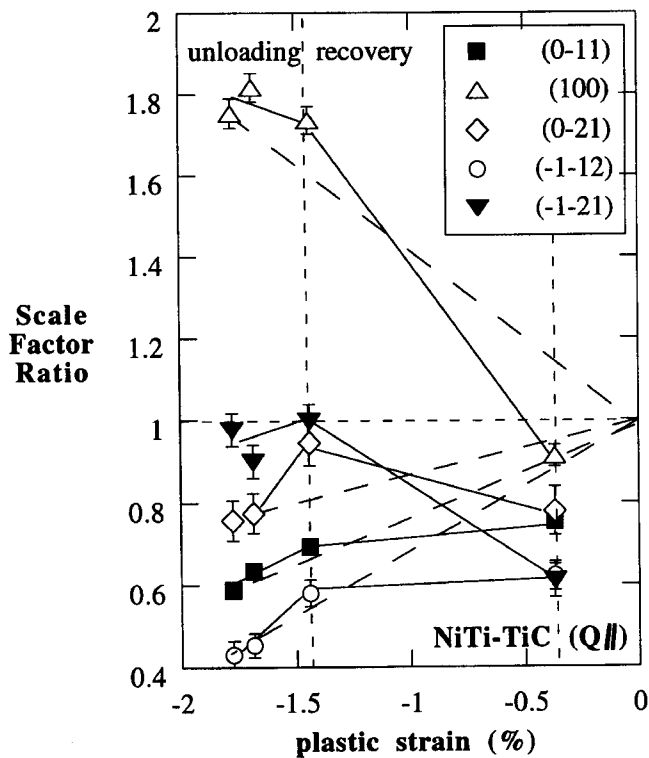
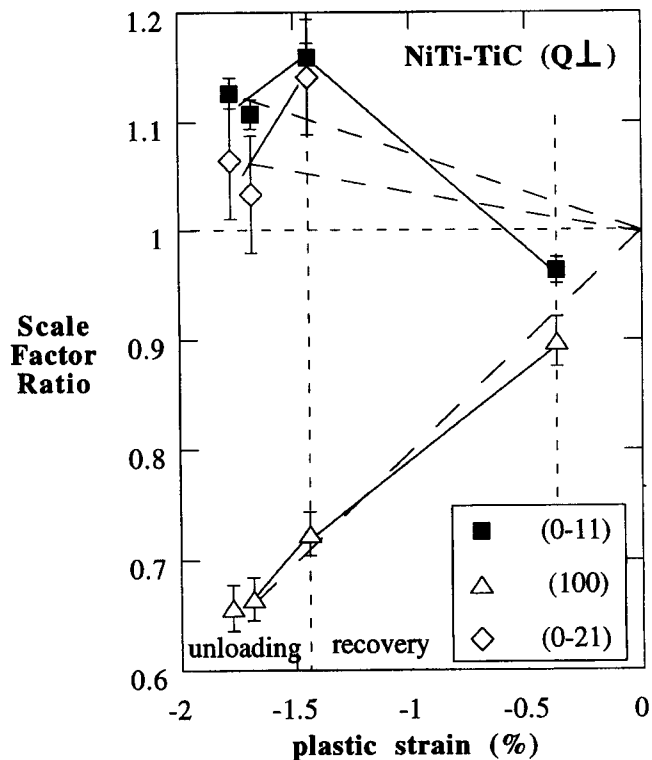


Fig. 6—Normalized scale factor upon mechanical unloading as a function of plastic strain for NiTi: (a) for planes perpendicular to the applied stress (-90 deg); and (b) for planes parallel to the applied stress ($+90$ deg).



(a)



(b)

Fig. 7—Normalized scale factor upon mechanical unloading as a function of plastic strain for NiTi-20TiC: (a) for planes perpendicular to the applied stress (-90°); and (b) for planes parallel to the applied stress ($+90^\circ$).

which is further discussed subsequently, may thus explain the low apparent elastic modulus of the composite at low strains. At large strains, localized twinning does not preclude the possibility of load transfer from the compliant matrix to the stiff reinforcement, as discussed in the following.

Neutron diffraction is well suited for the investigation of residual stresses and load transfer between phases in composites, because it allows the simultaneous and independent measurement of internal strains in matrix and reinforcement, as reported in aluminum matrix composites by References 17, 18, 37, and 38. In the following, we present and discuss our results for NiTi composites, for which, unlike aluminum composites, the matrix deforms by twinning rather than by slip. Comparing Figures 4(a) and (b), which display the lattice matrix elastic strains as a function of the applied stress, the elastic gradients for each of the planes are steeper for NiTi-20TiC (Figure 4(b)) than for NiTi (Figure 4(a)), with the possible exception of planes $(-1 \ -1 \ 2)$, for which large measurement errors exist. This behavior indicates that, for a given applied stress, the reinforced matrix carries proportionally less load than in unreinforced NiTi, *i.e.*, load transfer occurs between the matrix and reinforcement. Furthermore, for most of the planes, the elastic gradient becomes steeper at high stresses, as discussed later. To quantitatively compare our data to the predictions of elastic load transfer based on an Eshelby approach (Eqs. [B9] through [B12]), we used the TiC elastic constants,^[35] the $(1 \ 0 \ 0)$ elastic gradient determined above for NiTi, and two elastic constants determined by Brill *et al.*^[30] (Appendix A) and assumed that all other elastic constants of both

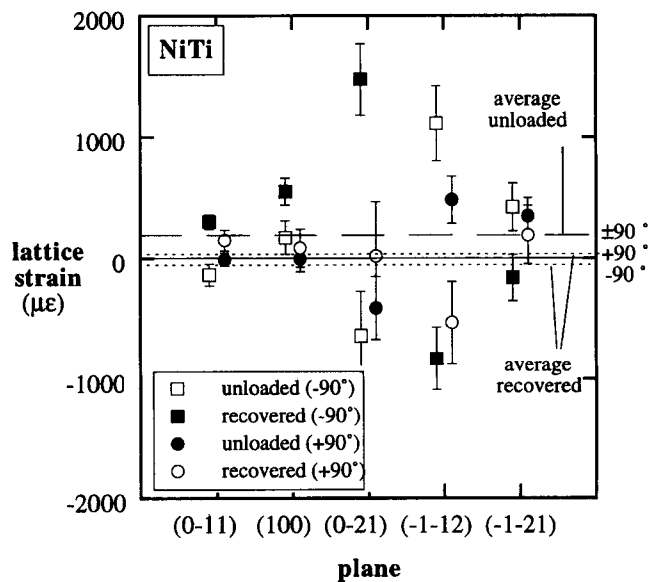


Fig. 8—Residual strain measured by neutron diffraction for NiTi after mechanical unloading (empty symbols) and shape-memory recovery (filled symbols) for planes perpendicular to the applied stress (-90°) and for planes parallel to the applied stress ($+90^\circ$). Average values are determined from the average of the strains in three cell directions calculated by Rietveld refinement.

NiTi and TiC can be calculated with an isotropic assumption.

Figure 10(a) shows the elastic behavior of the $(1 \ 0 \ 0)$ planes, for which the measurement error is small and the

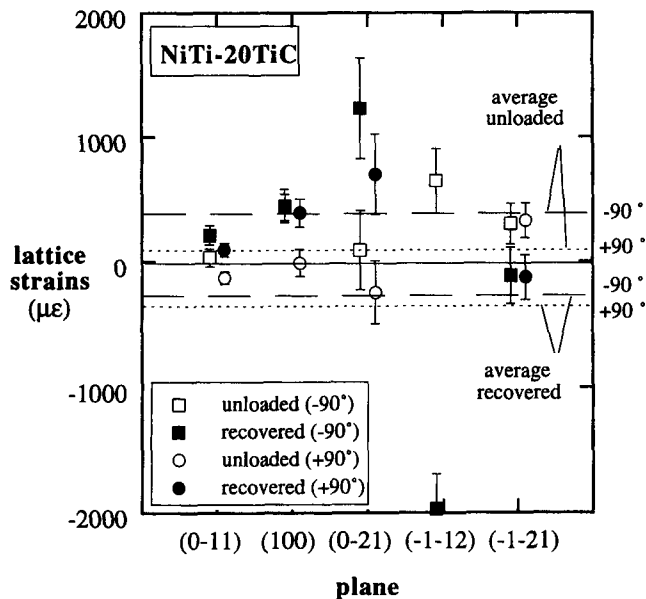


Fig. 9—Residual strain measured by neutron diffraction for NiTi-20TiC after mechanical unloading (empty symbols) and shape-memory recovery (filled symbols) for planes perpendicular to the applied stress (-90°) and for planes parallel to the applied stress ($+90^\circ$) (plane $(-1 -1 2)$ could not be measured due to peak overlap). Average values are determined from the average of the strains in three cell directions calculated by Rietveld refinement.

elastic gradient can be assimilated to $1/S_{11}$. For both directions parallel and perpendicular to the applied load, good agreement is found between the measured data and the predicted elastic behavior of the matrix. The matrix lattice strain for the highest applied stress seems to be slightly lower than expected if elastic load transfer is solely taking place. This indicates that additional load transfer may be taking place, as discussed later. Figure 10(b) shows the predictions for the TiC phase in the NiTi-20TiC sample, which are also in satisfactory agreement with the measurement.

We thus conclude that, while elastic load transfer is taking place in the NiTi-TiC composite in quantitative agreement with predictions by the Eshelby theory (Figures 10(a) and (b)), no macroscopic stiffening is observed in the apparent elastic region of the stress-strain plot (Figure 3 and Table I), as a result of the enhanced matrix twinning resulting from the mismatching particles.

B. Twinning Deformation

1. NiTi

The linear relationship shown in Figures 5(a) and (b) between the plastic strain and the scale factor ratio is found for all planes except $(0 -2 1)$, indicating that the main deformation mechanism is martensite variant coalescence, *i.e.*, twinning. In the direction of the applied load (Figure 5(a)), the scale factor ratio of $(1 0 0)$ increases, while those of $(0 -1 1)$ and $(-1 -1 2)$ decrease and those of $(0 -2 1)$ and $(-1 -2 1)$ are virtually unchanged. In the direction perpendicular to the applied load (Figure 5(b)), the opposite behavior is observed. Figures 5(a) and (b) thus indicate that twinning occurs such that martensitic variants with $(1 0 0)$ planes perpendicular to the applied load grow at the expense of those variants with $(0 -1 1)$ and $(-1 -1 2)$ planes perpendicular to the applied load. The increase of volume fraction of variants with $(1 0 0)$ planes perpendicular to the

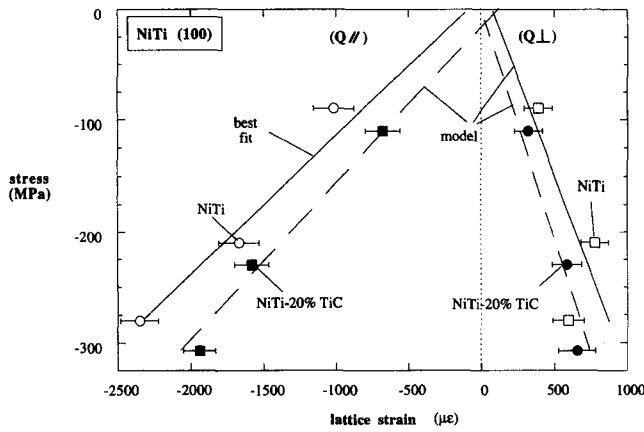
Table III. Predicted Mean Internal Stress $\bar{\sigma}$ and Mean Internal Strain $\bar{\epsilon}$ for NiTi (Matrix M) and TiC (Inclusion I) at Room Temperature Due to Thermal Mismatch and Transformation Mismatch between the Two Phases of NiTi-20TiC (Equations [B1] through [B8])

	$\bar{\sigma}_M$ (MPa)	$\bar{\sigma}_I$ (MPa)	$\bar{\epsilon}_M$ ($\cdot 10^6$)	$\bar{\epsilon}_I$ ($\cdot 10^6$)
Thermal mismatch	75	-302	182	-416
Transformation mismatch	-22	89	-54	123
Total mismatch	53	-213	128	-293

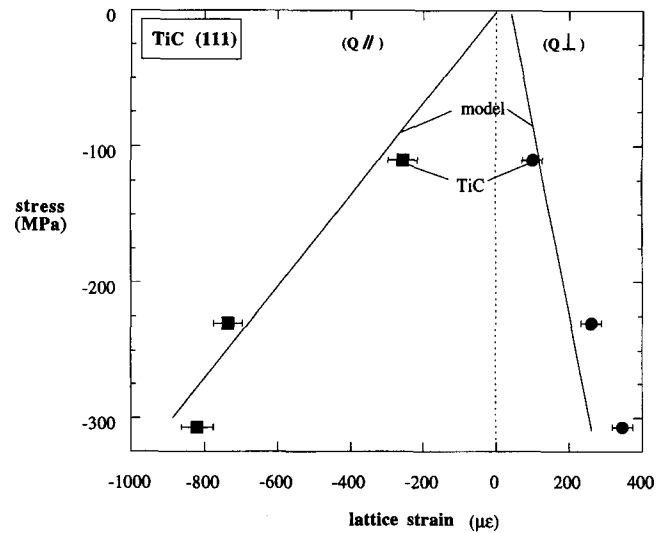
load is significant (about 70 pct, assuming that the scale factor ratio in Figure 5(a) is proportional to the fraction of variants contributing to diffraction); respectively, the decrease of variants with $(1 0 0)$ planes parallel to the load direction is about 20 pct (Figure 5(b)).

Two types of twinning have been reported for martensitic NiTi:^[39] type I twinning, with a mirror reflection about the twinning plane $K_1 = (1 1 -1)$;^[40] and type II twinning, with twinning plane $K_1 = (0.7205 1 -1)$, leading to a rotation by 180° around the shear direction $\eta = [0 -1 1]$.^[41,42] In the stereographic projection of Figure 11, the effect of $(1 1 -1)$ type I twinning and subsequent variant reorientation is given for planes $(1 0 0)$ and $(0 -1 1)$. It is apparent that, for the monoclinic structure of NiTi, plane $(1 1 -1)$ is close to being the bisector of planes $(1 0 0)$ and $(0 -1 1)$, which are almost orthogonal to each other. As shown in Figure 11 for $(1 1 -1)$ type I twinning, variants with $(1 0 0)$ planes parallel to the load axis (in Bragg's condition for the $+90^\circ$ deg detector) twin such that their $(1 0 0)$ planes are almost perpendicular to the load (in Bragg's condition for the -90° deg detector). Respectively, variants with $(0 -1 1)$ plane normal forming an angle of 8.4° deg with the loading direction twin such that their $(0 -1 1)$ planes are perpendicular to the load (in Bragg's condition for the $+90^\circ$ deg detector). The increase (respectively, decrease) upon mechanical loading of the $(1 0 0)$ scale factor ratio measured on the -90° deg detector (respectively, $+90^\circ$ deg detector) and the opposite behavior of the $(0 -1 1)$ scale factor ratio in Figure 5(a) (respectively, Figure 5(b)) can thus be explained satisfactorily by type I twinning about the $(1 1 -1)$ plane. On the other hand, type II twinning cannot justify the observed behavior, because planes $(1 0 0)$ and $(0 -1 1)$, which are perpendicular to $[011]$, should be rotated by 180° upon twinning, giving an equivalent diffraction orientation.

We expect that twinning is favored for variants with a maximum Schmid factor, *i.e.*, for variants with both the twinning plane K_1 and the shear vector η_1 (using the notation by Bilby and Crocker^[43]) forming a 45° angle with the load axis. With the twinning configuration calculated by Knowles and Smith^[44] ($K_1 = (1 1 -1)$, $\eta_1 = [0.54043 0.45957 1]$, $K_2 = (0.24694 0.50611 1)$, and $\eta_2 = [-2 -1 1]$), such a condition cannot be fulfilled in the configuration of Figure 11. Assuming the twinning plane $(1 1 -1)$ at an angle $\alpha = 45^\circ$ with the load axis, the angle between η_1 and the load axis is $\beta = 71.1^\circ$, which results in a Schmid factor $F = |\cos(\alpha) \cos(\beta)| = 0.21$. It is possible that twinning with a higher Schmid factor occurs for higher index planes but cannot be observed because of the low diffraction intensity of these planes.



(a)



(b)

Fig. 10—Measured elastic gradients: (a) NiTi lattice strains for NiTi and NiTi-20TiC for (1 0 0) in both directions. Linear regression fits are shown as full lines, and predicted behavior from the Eshelby's method (Eqs. [B3], [B4], [B9], [B11], and [B12]) is shown as dotted lines. The lines are not forced through the origin, thus taking into account a possible error at zero stress; and (b) (1 1 1) TiC lattice strains for NiTi-20TiC predicted behavior from the Eshelby's method is shown as full lines.

The preceding discussion considers a single crystal of austenite, which is transformed upon cooling into equal fractions of the 24 martensite variants. Upon straining, the variant leading to the largest strain is favored and the material deforms until that single variant has grown at the expense of all other variants. Upon heating above A_f , the monocrystalline martensitic sample can then be fully recovered to the original monocrystalline austenite shape. The situation for a polycrystalline austenitic sample is more complex, because the variants formed in each of the randomly oriented austenitic grains are expected to twin, so that the deformation is maximal for the direction of the applied stress according to the orientation of the austenitic grain. Furthermore, the twinning behavior is expected to be influenced by the condition of strain compatibility required between grains. Figures 5(a) and (b) show that there is, on average, a clear trend for some variants to form at the expense of others, despite the complexity of the strain state in the deformed polycrystalline sample.

Figure 11 depicts the case where twinning shear results in (1 0 0) planes perpendicular to the load. While a symmetric situation can also be envisaged, whereby (1 0 0) planes are positioned parallel to load after twinning, the former case can be justified by variant conversion during deformation, as shown in the following.

The shape change associated with the transformation from austenite to a martensite variant β is calculated according to the method described by Saburi and Nenno.^[2] Strains are calculated relative to the parent vector basis. The strain upon twinning from variant β_1 to variant β_2 (Table IV) is obtained as the difference between the strain from austenite A to β_1 and the strain from A to β_2 . Strains for β_1 - β_2 variant conversion for all correspondence variant combinations for (1 1 -1) type I twinning^[45] are listed in Table V, as projected along three of the main austenite directions. By comparing correspondence variants (Table IV) and strains along (1 0 0)_{B2} (Table V), it is apparent that correspondence of [100]_M with (1 0 0)_{B2} given by variant

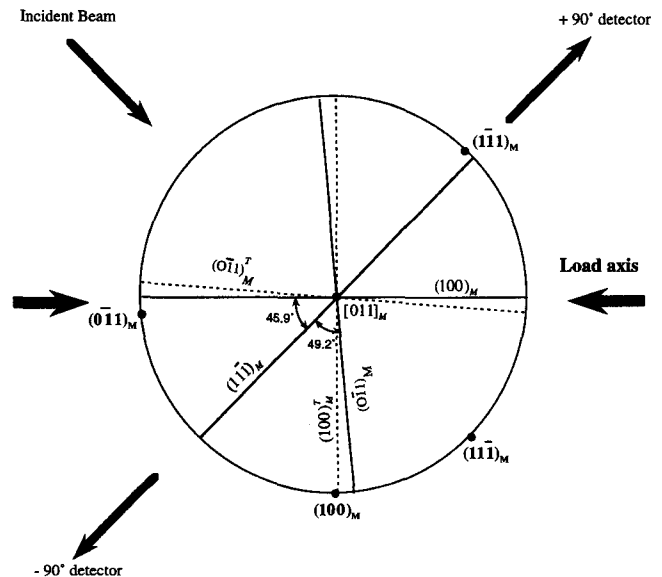


Fig. 11—Stereographic projection along $[0 1 1]_M$ showing positions of $(0 -1 1)_M$ and $(1 0 0)_M$ before (full line) and after (dotted line) type I (1 1 -1) twinning. The twinned (1 0 0) planes are in diffraction position. Poles are indicated in bold type and plane position after twinning with the superscript T .

conversion to 1, 1', 2, and 2' yields a negative compressive strain of -6.8 pct. It can also be verified from Table V that the preceding variant conversions give a correspondence between $[0 -1 1]_M$ and $(0 1 0)_{B2}$. Therefore, compression of crystals having a parent phase with one of the cubic cell axes lying close to the load axis is likely to show alignment of $[100]_M$ with the load axis. On the other hand, $[0 -1 1]_M$ will tend to lie perpendicularly to the load axis. Such correspondences are also likely with vectors of reciprocal lattice $(1 0 0)_M$ and $(0 -1 1)_M$, as the angle between $[100]_M$ and $(1 0 0)_M$ and between $[0 0 1]_M$ and $(0 0 1)_M$ is small ($\alpha = 7.8$ deg) and $[0 1 0]_M$ is parallel to $(0 1 0)_M$. Therefore, a configuration with (1 0 0) martensite planes perpendicular

Table IV. Austenite (B_2)-Martensite (M) Lattice Correspondence

Variant	[1 0 0] _M	[0 1 0] _M	[0 0 1] _M
1	[1 0 0] _{B2}	[0 1 1] _{B2}	[0 -1 1] _{B2}
1'	[-1 0 0] _{B2}	[0 -1 -1] _{B2}	[0 -1 1] _{B2}
2	[1 0 0] _{B2}	[0 -1 1] _{B2}	[0 -1 -1] _{B2}
2'	[-1 0 0] _{B2}	[0 1 -1] _{B2}	[0 -1 -1] _{B2}
3	[0 1 0] _{B2}	[-1 0 1] _{B2}	[1 0 1] _{B2}
3'	[0 -1 0] _{B2}	[1 0 -1] _{B2}	[1 0 1] _{B2}
4	[0 1 0] _{B2}	[1 0 1] _{B2}	[1 0 -1] _{B2}
4'	[0 -1 0] _{B2}	[-1 0 -1] _{B2}	[1 0 -1] _{B2}
5	[0 0 1] _{B2}	[1 -1 0] _{B2}	[1 1 0] _{B2}
5'	[0 0 -1] _{B2}	[-1 1 0] _{B2}	[1 1 0] _{B2}
6	[0 0 1] _{B2}	[1 1 0] _{B2}	[-1 1 0] _{B2}
6'	[0 0 -1] _{B2}	[-1 -1 0] _{B2}	[-1 1 0] _{B2}

Table V. Variant Conversion Strain (Percent) Calculated Along the Three Main Directions of the Parent Phase

Variant Combination	(1 0 0) _{B2}	(1 1 0) _{B2}	(1 1 1) _{B2}
3' \Rightarrow 1	-6.8	0.0	-13.4
6' \Rightarrow 1	-6.8	6.9	0.0
5' \Rightarrow 1'	-6.8	-13.6	-13.4
4 \Rightarrow 1'	-6.8	0.0	0.0
6 \Rightarrow 2	-6.8	6.9	13.4
4' \Rightarrow 2	-6.8	0.0	13.4
3 \Rightarrow 2'	-6.8	0.0	0.0
5 \Rightarrow 2'	-6.8	-13.6	0.0
5 \Rightarrow 3	0.0	-13.6	0.0
6' \Rightarrow 3'	0.0	6.9	13.4
5' \Rightarrow 4	0.0	-13.6	-13.4
6 \Rightarrow 4'	0.0	6.9	0.0

to the load and (0 -1 1) planes parallel to the load is favorable for compression. Due to diffraction geometry, only planes parallel or perpendicular to the load axis are detected. Some other variant conversions are likely to be observed giving even larger strains. In particular, for crystals with a parent phase with (1 1 1)_{B2} axis parallel to the sample axis, an increase of (1 1 0)_M scale factor ratio (due to conversion 3' \rightarrow 1, 5' \rightarrow 1', and 5' \rightarrow 4) should be observed, because the compressive strain is important in that direction (-13.4 pct). However, the corresponding diffraction peak is very weak and little change can be detected in the spectra. Finally, compression of crystals with a parent phase with (1 1 0)_{B2} axis parallel to the sample should affect the scale factor ratio of (2 1 -1)_M by variant conversion 5' \rightarrow 1' (strain of -13.6 pct), as qualitatively observed in the diffraction spectra. Again, the effect is difficult to measure due to the weak peak intensity.

2. NiTi-TiC

Plastic deformation of the matrix in the presence of elastic particles results in a plastic mismatch which is additive to the elastic mismatch contribution. Thus, load transfer should be enhanced compared to a case where both phases are elastic, with a concomitant increase in the gradient of the applied stress vs the lattice strain curve of the matrix (Figures 4(a) and (b)). Respectively, a decrease is expected for the elastic gradient of the reinforcement. These effects were observed by neutron diffraction in metal matrix composites deforming plastically by slip.^[29,37] In the case of NiTi-20TiC deforming by twinning, these effects are much less than predicted by Eqs. [B9] through [B12], indicating that, unlike composites deforming by slip, NiTi-20TiC deforming by twinning relaxes very efficiently the plastic mismatch between the matrix and reinforcement. As seen in Figure 4(b), no significant deviation of the elastic gradient is observed in the NiTi matrix up to an applied stress of -230 MPa (corresponding to a macroscopic plastic strain of -0.81 pct), except possibly for a small deviation for plane (0 -1 1). Upon further increase of the applied stress to -310 MPa (corresponding to more than a doubling of the plastic strain to a value of -1.78 pct), the expected deviations from the elastic line are found for the (0 -1 1), (0 -2 1), and (-1 -1 2) planes and possibly (-1 -2 1)

(Figure 4(b)). This may indicate a threshold stress, above which variants with these planes perpendicular to the load become unstable and twin. However, no measurable deviation is observed for the NiTi (1 0 0) planes perpendicular to the applied stress (Figure 10(a)) or for the TiC particles (Figure 10(b)). While the measurement resolution is comparable to the small deviation expected for the TiC, the lack of plastic load transfer for the NiTi (1 0 0) planes perpendicular to the applied load is puzzling. A possible explanation may be that plastic load transfer takes place concurrently with the decrease of the fraction of the unstable variants. NiTi variant conversion may thus minimize load transfer to the TiC particles and to the matrix stable variants ((1 0 0) planes perpendicular to the load axis) as the fraction of the unstable variants decreases upon loading.

These *in situ* elastic measurements (Figures 4(b) and 10(a) and (b)), the *in situ* orientation measurements (Figures 5(a) and (b)) discussed earlier, and the overlapping stress-strain plot (Figure 3) all indicate that the addition of 20 vol pct TiC particles has little effect on the plastic behavior of the matrix over the strain range explored here. This is in sharp contrast with the marked strengthening, increased rate of strain hardening, and increased plastic load transfer between the matrix and reinforcement observed in metal matrix composites with a matrix plastically deforming by slip.^[27,29] The insensitivity of the NiTi matrix to the presence of a large volume fraction of stiff, mismatching particles can be interpreted as the result of the greater ease for mismatch relaxation by twinning, as compared to slip. In the latter case, accommodation takes place by dislocation punching, which results in strain hardening of the matrix and concomitant increase in strength.^[46,47] In contrast, for martensitic NiTi, complete relaxation of the mismatch between the elastic particle and the plastic matrix is possible by local twinning. This is illustrated schematically in Figure 12, for a two-dimensional crystal with four possible variants. If the crystal contains a hole and is deformed by twinning from variant C to variant A, a concomitant change in the shape of the hole results. However, if the hole contains a rigid particle and the crystal is again twinned from variant C to variant A, complete accommodation of the resulting mismatch is possible by retaining some of the variant C in contact with the particle and accommodating the A-C

boundary by a *B* twin (Figure 12(b)). Figure 2(b) shows an example of such accommodation twins. The net result is an overall macroscopic deformation similar to that of the particle-free case (Figure 12(a)), with a small volume fraction of accommodating variants (*B* and *C* in Figure 12(b)). Such a mechanism requires that variants (*B*) be twin related with two other variants. Variant correspondence combinations in Table V indicate that such a configuration is possible for (1 1 -1) type I twinning: for example, variant 1 is twin related to variants 3' and 6'. Because such accommodating variants are expected to also exist for particle-free, polycrystalline NiTi to relax mismatch between grains of different orientations, the twins necessary to accommodate elastic particles in a polycrystalline composite sample may represent only a small fraction of the twins already existing in particle-free polycrystalline samples. This hypothesis explains the lack of significant difference between NiTi and NiTi-20TiC in terms of macroscopic behavior (Figure 3) and average variant orientation by twinning (Figures 5(a) and (b)). Furthermore, unlike relaxation by slip, no strain hardening is expected as a result of localized twinning relaxing the mismatch.

C. Deformation upon Mechanical Unloading

1. NiTi

The apparent Young's modulus measured by strain gage upon mechanical unloading ($E = 61 \pm 4$ GPa) is lower but comparable to that upon loading ($E = 69 \pm 4$ GPa), but significantly lower than the value calculated in Appendix A from diffraction data ($\bar{E} = 76$ GPa). Two explanations can be given for this discrepancy, both based on the high anisotropy of NiTi elastic constants (Figures 4(a) and (b)). First, twinning may take place immediately upon mechanical unloading of the sample, as a result of internal mismatch stresses between variants with different spatial orientations. Figures 6(a) and (b) indeed indicate that twinning takes place upon unloading at a nominal applied stress of -100 MPa. This behavior is similar to the Bauschinger effect for slip: as the external stress is reversed, those dislocations, for which the total stress (the sum of the external and internal stresses) exceeds the Peierls stress, start to glide. The result is, as observed for NiTi (Figure 3), reverse yield upon mechanical unloading and a low apparent Young's modulus. Second, the low unloading Young's modulus may also be the result of orientation of compliant variants by twinning during mechanical loading: this is consistent with the observation that (1 0 0) planes are oriented perpendicularly to the stress axis after deformation (Figure 5(a)), if $E_{(100)}$ is lower than average, as suggested by the low elastic gradient of (1 0 0) planes in Figure 4(a).

As shown in Figure 3, the anelastic recovery increases nonlinearly with decreasing load, resulting in a measurable departure from the apparent elastic line at a stress of about -160 MPa (Table I). Such nonlinear recovery in shape-memory alloys—variously called rubberlike, ferroelastic, or anelastic behavior^{2,6}—was observed in NiTi for both tension and compression⁴⁸ and is usually attributed to variant reverse twinning. Figures 6(a) and (b) indicate that reverse twinning is indeed taking place upon mechanical unloading. However, the behavior is not reversible with respect to loading (as shown with dotted lines in Figures 6(a) and (b)): upon mechanical unloading to -3 MPa, (1 0 0) planes de-

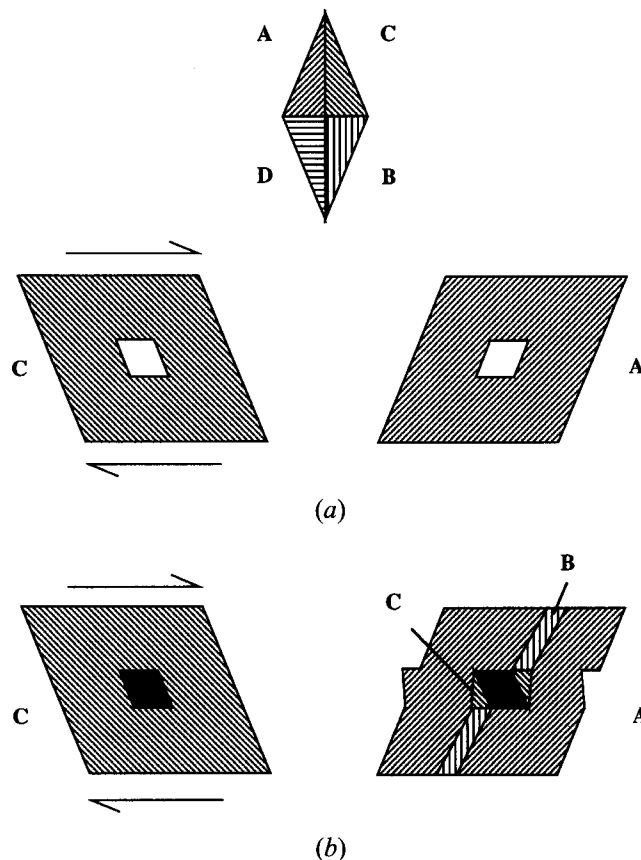


Fig. 12—Two-dimensional illustration of the accommodation of a mismatching rigid particle within a martensitic crystal with four possible variants *A*, *B*, *C*, and *D*: (a) crystal with orientation *C* containing a hole, deformed by twinning to orientation *A*; and (b) crystal with orientation *C* containing a rigid particle, deformed by twinning to orientation *A* with accommodation twins *C* and *B* for the undeformed particle.

twin more readily than they twinned upon loading, while the twinning behavior upon unloading of the other planes in Figure 6(a) is not correlated to that upon loading. The same lack of correlation is found for the twinning behavior upon unloading in the direction perpendicular to the applied stress (Figure 6(b)).

We note that a reversible behavior is not expected, because the stress state at a given strain is very different upon mechanical loading and unloading. Rather, the NiTi twinning behavior upon unloading can be interpreted in terms of minimization of elastic residual stresses. As these mismatch stresses increase upon mechanical unloading because of misfit between variants with anisotropic elastic moduli (Figures 4(a) and (b)), twinning takes place as a relaxation mechanism. However, as shown in Figure 8, the residual strains for the direction parallel to the applied stress are inhomogeneous after complete mechanical unloading: they vary from near 0 pct for (0 -1 1) and (1 0 0) to about $\epsilon = 0.1$ pct for (-1 -1 2). Residual strains in the direction perpendicular to the load (Figure 8) exhibit similar signs and magnitudes, indicating that the residual stress state is likely to exhibit a significant hydrostatic component. We note that, because twinning operates without volume change, hydrostatic stresses cannot be eliminated by this deformation mechanism. Average residual strains calculated from the average of the values in the three cell directions (Table II) are zero, within experimental error: $\epsilon =$

$1.4 \cdot 10^{-4}$ and $\epsilon = 1.2 \cdot 10^{-4}$ parallel and perpendicular to the stress axis, respectively (Figure 8). We, however, recall that these residual strains are not absolute values but are differences with respect to the undeformed material, which may also have displayed nonzero internal strains as a result of the phase transformation upon cooling (Table III). These strains, however, are expected to be small as a result of the self-accommodating nature of the martensitic transformation.

2. NiTi-TiC

As is the case for NiTi, the apparent Young's moduli of NiTi-20TiC measured by strain gages are similar for both loading and unloading and are significantly smaller than the value calculated assuming elastic load transfer. This indicates that twinning occurs as soon as the mechanical load is removed, and as discussed previously for the case of loading that the TiC particles stimulate twinning, as a result of elastic and plastic mismatches between the matrix and particles on unloading.

The NiTi-TiC composite exhibits rubberlike behavior upon mechanical unloading, leading to an anelastic strain similar to that of NiTi after full unloading (Table I). As for NiTi, substantial detwinning upon mechanical unloading is responsible for this behavior, as shown in Figures 7(a) and (b). While the macroscopic behavior is similar to that of NiTi (Figure 3), a comparison of Figures 6(a) and (b) and 7(a) and (b) shows that detwinning upon unloading is different in NiTi and NiTi-20TiC for each of the planes: the effect is particularly evident for planes (1 0 0) in Figures 6(a) and 7(a) and for planes (0 -1 1) in Figures 6(b) and 7(b). This is in contrast to the case of loading, for which a similar twinning behavior is observed for NiTi and NiTi-20TiC for almost all planes (Figures 5(a) and (b)). While the two samples are not directly comparable upon unloading because they have been strained to different values before unloading (-1.6 pct for NiTi and -2.0 pct for NiTi-20TiC), a comparison of Figures 6(a) and (b) and 7(a) and (b) shows that the extent of reverse twinning is systematically less marked for the composite than for the bulk material.

Figures 8 and 9, however, indicate that residual strains for all measured planes are similar for NiTi and NiTi-20TiC. The average residual strain calculated from the three cell directions (Table II) is also very small: $\epsilon = 3.1 \cdot 10^{-4}$ and $\epsilon = 7 \cdot 10^{-5}$ parallel and perpendicular to the stress axis, respectively (Figure 9). Negligible residual strains are also found in the TiC particles: $\epsilon = 2.5 \cdot 10^{-5}$. This indicates again that the matrix is minimizing its internal strain energy upon unloading, rather than twinning in a reversible manner. This also confirms that the TiC particles have little effect upon the residual strain state of the matrix, most probably as a result of the ease of relaxation by twinning described earlier (Figure 12). As already pointed out for the case of mechanical loading, this behavior is in contrast to that of metal matrix composites deforming by slip, whereby particles strongly influence the residual stress state of the matrix.

D. Shape-Memory Recovery

1. NiTi

As a result of heating the deformed specimen above the A_s temperature and cooling again to room temperature, 77

pct of the permanent strain resulting from compressive deformation is recovered (Table I). The lack of complete recovery can be attributed to plastic deformation by slip of the material, as investigated and discussed in part III of this article series.^[11] Figures 6(a) and (b) show the scale factor ratios before and after shape-memory recovery. In the direction of mechanical loading (Figure 6(a)), most variants have recovered, so as to partially cancel the preferred orientation induced by mechanical deformation. Figure 6(b) also indicates that the preferred orientation is not fully recovered in the direction perpendicular to the mechanical loading. While the orientation of the 24 variants can be considered random after hot pressing of powders, the preceding results indicate that thermal cycling above the transformation temperature does not fully eliminate the preferred orientation introduced by deformation. This result is important, because many studies have used deformed samples (swaged wires, rolled plates, etc.), the deformation history and texture of which are likely to affect their subsequent mechanical properties.

Figure 8 shows that, while the sign of the residual strains varies in most cases before and after shape-memory recovery for a given plane, their magnitude is similar for each plane family. Some planes exhibit a small increase in residual strains while others show a small decrease, on the order of 0.03 pct. The average strains (Table II) in both directions are zero within experimental error. This behavior confirms that self-accommodation during martensitic transformation effectively minimizes the residual stresses after transformation.

In summary, Figures 6(a) and (b) and 8 illustrate that upon shape-memory recovery of NiTi, the preferred orientation is only partially recovered while the internal stresses are minimized.

2. NiTi-TiC

TiC particles do not significantly interfere with the shape-memory effect. First, as shown in Table I, the fraction of strain recovered by shape-memory heat treatment is only slightly smaller for NiTi-20TiC than for NiTi. This result confirms that the mismatching TiC particles do not induce a significant amount of slip in the material during deformation, since the strain resulting from slip is unrecoverable. Second, comparison of Figures 6(a) and (b) and Figures 7(a) and (b) shows that the preferred variant orientation after shape-memory recovery is similar for both materials, despite the differences in variant orientation before shape-memory recovery. Third, the signs and amplitude of the residual strains for all planes (except plane (-1 -1 2)) are, within experimental error, the same for both materials, as shown in Figures 8 and 9. As for NiTi, the average residual strain (Table II) is low in the NiTi-TiC composite: $\epsilon = -2.3 \cdot 10^{-4}$ and $\epsilon = -3.7 \cdot 10^{-4}$ parallel and perpendicular to the stress axis, respectively (Figure 9).

If martensite deformation occurs purely by twinning of variants, which also accommodates the mismatch of TiC particles, as depicted in Figure 12, transformation to austenite after twinning is indeed expected to be mostly unaffected by the TiC particles. Upon heating to a temperature above A_s , the composite is returned to the same state as before deformation, for which, as shown earlier, little thermal mismatch strains are expected. Subsequent cooling to room temperature induces again small transformation mis-

match strains, which can be minimized by self-accommodation through an appropriate combination of variants at the interface, similarly to the case of strain-induced deformation illustrated in Figure 12(b).

V. SUMMARY

The study by neutron diffraction of martensitic NiTi subjected to uniaxial, compressive deformation up to a strain of -1.6 pct and subsequent mechanical unloading and shape-memory recovery leads to the following conclusions.

1. The elastic crystallographic gradients E_{hkl} measured by diffraction indicate that NiTi is elastically very anisotropic. Using E_{100} and two elastic constants obtained from ultrasonic measurements by Brill *et al.*,^[30] an average modulus $\bar{E} = 76$ GPa is calculated. This value is higher than those obtained by strain gages upon initial loading ($E = 69$ GPa) and upon unloading ($E = 61$ GPa). A possible explanation for this discrepancy is the occurrence of twinning below the apparent macroscopic yield stress, as a result of mismatch accommodation between martensitic variants with anisotropic elastic properties.
2. Diffraction intensity results show that twinning occurs by variant reorientation by $(1\ 1\ -1)$ type I twinning in the plastic region of the stress-strain plot. Variant reorientation increases linearly with increasing plastic strain: variants with $(1\ 0\ 0)$ planes perpendicular to the loading axis are favored at the expense of those with $(0\ -1\ 1)$ and $(-1\ -1\ 2)$ planes perpendicular to the loading axis; the opposite behavior is observed perpendicular to the loading axis. Computation of the average shape strains shows that this orientation is favored in compression, since it results in an average contraction of -6.8 pct.
3. Upon mechanical unloading, deviation from the apparent elastic line is observed. This rubberlike behavior is the result of reverse twinning upon unloading, which is not reversible with respect to strain and stress, leading to an orientation state different from that during deformation. Rather, reverse twinning occurs such that average residual strains after unloading are very low, minimizing the mismatch between variants with anisotropic elastic constants.
4. Shape-memory heat treatment results in a recovery of 70 pct of the deformation and partial recovery of the preferred orientation developed during deformation. Residual strains after recovery are negligible, as a result of self-accommodation upon martensitic transformation.

The following conclusions are drawn from the investigation of martensitic NiTi containing 20 vol pct TiC particulates deformed up to a strain of -2 pct.

1. The Eshelby theory predicts low residual stresses, resulting from thermal and transformation mismatch between the matrix and reinforcement upon cooling from processing temperature. Diffraction measurements support that prediction and thus confirm that self-accommodation occurs in the bulk during the allotropic transformation, minimizing internal strains resulting from the large orientation and shape mismatch between individual martensitic variants and TiC particles.
2. The macroscopic Young's modulus measured by strain

gages is not increased by the stiff TiC particulates, in disagreement with predictions from the Eshelby theory. This indicates that the elastic mismatch between the matrix and particles enhances twinning below the apparent yield stress.

3. Elastic load transfer is taking place between the compliant matrix and the stiff particles during both elastic and plastic deformation of the composite, in satisfactory agreement with quantitative predictions from the Eshelby's theory for elastic mismatch.
4. Upon plastic deformation of the composite by matrix twinning, little plastic load transfer between the two phases is observed in addition to the preceding elastic load transfer. Furthermore, the TiC particles have little effect on the macroscopic plastic behavior of the matrix or on the volume fractions of twinned variants. These observations indicate that the plastic mismatch between the matrix and reinforcement is very efficiently relaxed by localized matrix twinning. The overall composite behavior is quite similar to that of bulk NiTi, in sharp contrast to metal matrix composites deforming by slip, for which plastic mismatch results in an increased work-hardening rate.
5. As for mechanical loading, the Young's modulus upon unloading is lower than expected, indicating that twinning occurs as a result of the elastic incompatibility between the two phases. The total rubberlike strain recovered upon unloading is similar to that of unreinforced NiTi, and the residual strains are low, indicating that the TiC particles do not prevent the matrix from minimizing its elastic energy.
6. Shape-memory heat treatment results in a behavior very similar to that of bulk NiTi, indicating that the mismatch from the particles is completely canceled by self-accommodation during the phase transformations. As a result, the shape-memory recovery capability of NiTi is mostly unaffected by the presence of 20 vol pct TiC particles.

ACKNOWLEDGMENTS

The Manuel Lujan, Jr. Neutron Scattering Center is a national user facility funded by the United States Department of Energy, Office of Basic Energy Science; this work was supported in part by DOE Contract No. W-7405-ENG-36. DM and DCD also acknowledge the support of the Swiss National Foundation, in the form of a postdoctoral grant, and of AMAX, in the form of an endowed chair at MIT. The authors would like to thank Ms. K.L. Fukami-Ushiro from MIT for sample preparation, Mr. L. Bataillard from EPFL (Switzerland) for electron microscopy, and Dr. A. Lawson from LANL for helpful discussions.

APPENDIX A

NiTi average Young's modulus

Neutron measurements of elastic constants E_{hkl} do not allow obtainment of average elastic constants of the material, because shear constants such as C_{44} are not measurable. In the following, we calculate the average Young's mod-

ulus of NiTi assuming a cubic structure and using our neutron diffraction measurements and two elastic constants (shear constant C_{44} and Poisson's ratio ν) determined by Brill *et al.*^[30] by ultrasonic measurements. These authors cooled an austenite single crystal below M_f and measured the elastic constants of the martensite as defined by the parent vector base. With the lattice correspondences of Table IV, all cube directions $[100]_{B_2}$, $[010]_{B_2}$, and $[001]_{B_2}$ correspond to $[100]_M$, which is close to $(1\ 0\ 0)_M$ in the martensite.

The constants C_{11} and C_{22} can be found by using the approximation for a cubic material:^[49]

$$C_{11} = \frac{S_{11} + S_{12}}{(S_{11} - S_{12})(S_{11} + 2S_{12})} \quad [A1]$$

$$C_{12} = \frac{-S_{12}}{(S_{11} - S_{12})(S_{11} + 2S_{12})} \quad [A2]$$

where

$$S_{11} = \frac{1}{E_{100}} \quad [A3]$$

$$S_{12} = -\nu S_{11} \quad [A4]$$

with $E_{100} = 125$ GPa, as determined from the slope of the best-fit line of the data in Figure 4(a), and $\nu = 0.35$, as determined by Brill *et al.*^[30]

The shear modulus $\bar{\mu}$ is calculated as an average of the Reuss and Voigt averages:^[13]

$$\bar{\mu} = \frac{1}{10} \left\{ (C_{11} - C_{12}) + 3C_{44} \right\} + 5 \left\{ 8(C_{11} - C_{12})^{-1} + 6C_{44}^{-1} \right\}^{-1} \quad [A5]$$

where $C_{44} = 20$ GPa, as measured by Brill *et al.*^[30] at 250 K, a temperature corresponding to the same undercooling below M_f as our sample at room temperature. Introducing Eqs. [A1] through [A4] into Eq. [A5] gives an average shear modulus $\bar{\mu} = 28.1$ GPa. The average Young's modulus is then

$$\bar{E} = 2(1 + \nu) \bar{\mu} \quad [A6]$$

yielding $\bar{E} = 76$ GPa. This value is much lower than any of the measured elastic gradients, as a result of the low value of C_{44} . For the same reason, the shear modulus calculated from the isotropic approximation

$$\mu = \frac{1}{2(S_{11} - S_{12})} \quad [A7]$$

gives a value $\mu = 46.3$ GPa, much higher than the value $\bar{\mu} = 28.1$ GPa found with Eq. [A5].

The previous results, however, are a rough approximation, due to the cubic assumption, the experimental errors in our neutron diffraction measurements, and the suitability of using the ultrasonic measurements of Brill *et al.*^[30]

APPENDIX B

Determination of internal mismatch stresses

In the following, we apply the equivalent homogenous inclusion model developed by Eshelby,^[50] who considered a random distribution of ellipsoidal inclusions in an isotro-

pic matrix, both phases exhibiting different elastic constants. We use the solutions for nondilute systems, described in more detail in References 29, 37, and 51.

A. Thermal and Transformation Mismatch Stresses

The equivalent transformation strain tensor ϵ^T is a function of the mismatch strain tensor ϵ^* between matrix m and inclusion i .

$$\epsilon^T = -\left\{ (C_m - C_i) \cdot [S - f(S - I)] - C_m \right\}^{-1} C_i \epsilon^* \quad [B1]$$

where f is the volume fraction of inclusions, I is the identity matrix, C is the stiffness tensor, and S is the Eshelby tensor:

$$S_{1111} = S_{2222} = S_{3333} = \frac{7 - 5\nu}{15(1 - \nu)} \quad [B2a]$$

$$S_{1122} = S_{2233} = S_{3311} = S_{1133} = S_{2211} = S_{3322} = \frac{5\nu - 1}{15(1 - \nu)} \quad [B2b]$$

$$S_{1212} = S_{2323} = S_{3131} = \frac{4 - 5\nu}{15(1 - \nu)} \quad [B2c]$$

which, for spherical particles, is only a function of the matrix Poisson's ratio ν . The matrix mean internal stress tensor $\langle \sigma \rangle_m$ and inclusion mean internal stress tensor $\langle \sigma \rangle_i$ can then be calculated from Eq. [B1] as

$$\langle \sigma \rangle_m = -f C_m (S - I) \epsilon^T \quad [B3a]$$

$$\langle \sigma \rangle_i = (1 - f) C_m (S - I) \epsilon^T \quad [B3b]$$

The corresponding mean internal strain tensors $\langle \epsilon \rangle$ for the matrix and inclusion are

$$\langle \epsilon \rangle_m = C_m^{-1} \langle \sigma \rangle_m \quad [B4a]$$

$$\langle \epsilon \rangle_i = C_i^{-1} \langle \sigma \rangle_i \quad [B4b]$$

and correspond to the average strains measured by neutron diffraction when no external load is applied on the composite.

We assume that the total mismatch resulting from cooling of the composite from annealing temperature to room temperature T_r is the sum of a thermal strain—resulting from the mismatch of coefficients of thermal expansion of matrix and inclusion—and a transformation strain—resulting from the phase transformation of the matrix in the presence of the nontransforming inclusions.

First, the linear thermal mismatch strain resulting from cooling from the annealing temperature to M_s is

$$\epsilon_{thA}^* = (\alpha_m - \alpha_i)(T_0 - M_s) \quad [B5]$$

where α_m is the austenitic matrix coefficient of thermal expansion, α_i is the inclusion coefficient of the thermal expansion, and T_0 is the temperature at which the mismatch between the two phases is zero, corresponding to the annealing temperature if no relaxation takes place during cooling from the annealing temperature. Because diffusion and creep processes are rapid above a homologous temperature of 0.65,^[52] we assume that all thermal mismatch stresses are relaxed at this temperature, corresponding to $T_0 = 756$ °C for equiatomic NiTi.^[53]

Second, the matrix allotropic transformation results in a linear expansion strain upon cooling from M_s to M_f :

$$\epsilon_{A-M}^* = \frac{1}{3} \frac{\Delta V}{V} \quad [B6]$$

where $\Delta V/V$ is the fractional constrained volume change

upon phase transformation and assuming that the phase transformation is purely hydrostatic in nature, *i.e.*, that all shear strains are zero on average. This is expected for a textureless polycrystal, where the shear strains resulting from the transformation of individual variants are canceled by self-accommodation.^[4] Third, the linear thermal mismatch strain resulting from cooling the martensitic composite from M_f to T_R is

$$\varepsilon_{ihM}^* = (\alpha_m' - \alpha_i) (M_f - T_R) \quad [B7]$$

where α_m' is the martensitic matrix coefficient of thermal expansion.

The total mismatch strain tensor ε^* is found by adding the contributions of Eqs. [B5] through [B7] written in the simplified matrix notation of Nye^[49] as

$$\varepsilon^* = (\varepsilon_{ihA}^* + \varepsilon_{A-M}^* + \varepsilon_{ihM}^*) [1, 1, 1, 0, 0, 0] \quad [B8]$$

and neglecting higher order terms.

B. Elastic and Plastic Mismatch

When an external stress σ^A is applied to the composite, further mismatch strains and stresses result from the difference in elastic and plastic response between the two phases. Upon elastic deformation of both phases of the composite, the equivalent transformation strain ε^T can be written as

$$\varepsilon^T = -\left\{ (C_m - C_i) \cdot [S - f(S - I)] - C_m \right\}^{-1} (C_m - C_i) C_m^{-1} \sigma^A \quad [B9]$$

If the matrix undergoes a uniform plastic strain ε^P in the direction of loading while the inclusion is still elastic, the equivalent transformation strain ε^T is

$$\varepsilon^T = \left\{ (C_m - C_i) \cdot [S - f(S - I)] - C_m \right\}^{-1} C_i \varepsilon^P \quad [B10]$$

This is equivalent to replacing the transformation strain ε^* in Eq. [B1] by a transformation strain $-\varepsilon^P$. Introduction of Eq. [B9] or [B10] into Eqs. [B3a], [B3b], [B4a], and [B4b] yields the mean internal stress $\langle \sigma \rangle$ and mean internal strain $\langle \varepsilon \rangle$ for each phase. The average stresses $\bar{\sigma}$ for the matrix and inclusion are then

$$\bar{\sigma}_m = \sigma^A + \langle \sigma \rangle_m \quad [B11a]$$

$$\bar{\sigma}_i = \sigma^A + \langle \sigma \rangle_i \quad [B11b]$$

from which the average strains $\bar{\varepsilon}$ for the matrix and inclusion can be calculated as

$$\bar{\varepsilon}_m = C_m^{-1} \bar{\sigma}_m \quad [B12a]$$

$$\bar{\varepsilon}_i = C_i^{-1} \bar{\sigma}_i \quad [B12b]$$

These average strains correspond to the experimentally measurable strains by diffraction. Finally, the Young's modulus of the composite E_c can be found as

$$E_c = \frac{\sigma^A}{\varepsilon_3^A + f\varepsilon_3^T} \quad [B13]$$

using Nye's notation,^[49] where

$$\varepsilon^A = C_m^{-1} \sigma^A \quad [B14]$$

REFERENCES

1. J. Perkins: *Met. Forum*, 1981, vol. 4, pp. 153-63.
2. T. Saburi and S. Nenno: in *Solid-Solid Phase Transformations*, H.I.

- Aaronson, D.E. Laughlin, R.F. Sekerka, and C.M. Wayman, eds., TMS-AIME, Warrendale, PA, 1982, pp. 1455-79.
3. K. Otsuka and K. Shimizu: *Int. Met. Rev.*, 1986, vol. 31, pp. 93-114.
4. K. Shimizu and T. Tadaki: in *Shape Memory Alloys*, H. Funakubo, ed., Gordon and Breach, New York, NY, 1987, pp. 1-60.
5. T. Honma: in *Shape Memory Alloys*, H. Funakubo, ed., Gordon and Breach, New York, NY, 1987, pp. 61-115.
6. C.M. Wayman and J.D. Harrison: *J. Met.*, 1989, vol. 41, pp. 26-28.
7. E. Hornbogen: in *Progress in Shape Memory Alloys*, S. Euken, ed., DGM, Oberursel, Germany, 1992, pp. 3-19.
8. C.M. Wayman: *MRS Bull.*, 1993, vol. 18, pp. 49-56.
9. D. Mari and D.C. Dunand: *Metall. Mater. Trans. A*, 1995, vol. 26A, pp. 2833-47.
10. K.L. Fukami-Ushiro, D. Mari, and D.C. Dunand: *Metall. Mater. Trans. A*, 1996, vol. 27A, pp. 183-191.
11. K.L. Fukami-Ushiro and D.C. Dunand: *Metall. Mater. Trans. A*, 1996, vol. 27A, pp. 193-203.
12. D. Mari, L. Bataillard, D.C. Dunand, and R. Gotthardt: *J. Phys IV*, 1995, vol. 5, pp. 659-664.
13. I.C. Noyan and J.B. Cohen: *Residual Stress*, Springer-Verlag, New York, NY, 1987, pp. 63-116.
14. M.T. Hutchings: in *Measurement of Residual and Applied Stress Using Neutron Diffraction*, M.T. Hutchings and A.D. Krawitz, eds., Kluwer, Dordrecht, 1992, pp. 3-18.
15. A.D. Krawitz: in *Measurement of Residual and Applied Stress Using Neutron Diffraction*, M.T. Hutchings and A.D. Krawitz, eds., Kluwer, Dordrecht, 1992, pp. 405-20.
16. G.E. Bacon: *Neutron Diffraction*, Oxford University Press, Oxford, United Kingdom, 1962, pp. 72-73.
17. M.A.M. Bourke, J.A. Goldstone, M.G. Stout, A.C. Lawson, and J.E. Allison: in *Residual Stresses in Composites: Measurement Modeling and Effects on Thermomechanical Behavior*, E.V. Barrera and I. Dutta, eds., TMS, Warrendale, PA, 1993, pp. 67-77.
18. M.A.M. Bourke, J.A. Goldstone, N. Shi, J.E. Allison, M.G. Stout, and A.C. Lawson: *Scripta Metall. Mater.*, 1993, vol. 29, pp. 771-76.
19. J.A. Goldstone: Los Alamos National Laboratory, Los Alamos, NM, private communication, 1990.
20. R.B. Von Dreele, J.D. Jorgensen, and C.G. Windsor: *J. Appl. Crystal.*, 1982, vol. 15, pp. 581-89.
21. A.C. Larson and R.B. Von Dreele: Los Alamos National Laboratory Report No. LA-UR 86-748, Los Alamos, NM, 1986.
22. C.M. Jackson, H.J. Wagner, and R.J. Wasilewski: NASA-SP 5110, 1972, p. 49.
23. *The CRC Materials Science and Engineering Handbook*, J. Shackelford and W. Alexander, eds., CRC Press, Boca Raton, FL, 1992, pp. 358-436.
24. Y. Kudoh, M. Tokohami, S. Miyazaki, and K. Otsuka: *Acta Metall.*, 1985, vol. 33, pp. 2049-56.
25. W. Bührer, R. Gotthardt, A. Kulik, and O. Mercier: *J. Phys.*, 1982, vol. 43, pp. 219-24.
26. A.A. Golestaneh and J.M. Carpenter: *Acta Metall. Mater.*, 1990, vol. 38, pp. 1291-1305.
27. J.W. Hutchinson and R.M. McMeeking: in *Fundamentals of Metal Matrix Composites*, S. Suresh, A. Mortensen, and A. Needleman, eds., Butterworth-Heinemann, Boston, MA, 1993, pp. 158-73.
28. P.E. McHugh, R.J. Asaro, and C.F. Shih: in *Fundamentals of Metal Matrix Composites*, S. Suresh, A. Mortensen, and A. Needleman, eds., Butterworth-Heinemann, Boston, MA, 1993, pp. 139-57.
29. T.W. Clyne and P.J. Withers: *An Introduction to Metal Matrix Composites*, Cambridge University Press, Cambridge, United Kingdom, 1993, pp. 44-165.
30. T.M. Brill, S. Mittelbach, W. Assmus, M. Mullner, and B. Luthi: *J. Phys.: Condens. Mater.*, 1991, vol. 3, pp. 9621-27.
31. S. Spinner and A.G. Rozner: *J. Acoust. Soc. Am.*, 1966, vol. 40, pp. 1009-15.
32. W. Bührer, R. Gotthardt, and M.S. Wechsler: in *Int. Conf. on Martensitic Transformations*, Japan Institute of Metals, Sendai, 1986, pp. 687-702.
33. D.C. Dunand: in *The Encyclopedia of Advanced Materials*, D. Bloor, R.J. Brook, M.C. Flemings, and S. Mahajan, eds., Pergamon Press, Elmsford, NY, 1994, pp. 1502-07.
34. M.A.M. Bourke, J.A. Goldstone, M.G. Stout, and A. Needleman: in *Fundamentals of Metal Matrix Composites*, S. Suresh, A. Mortensen, and A. Needleman, eds., Butterworth-Heinemann, Boston MA, 1993, pp. 61-80.
35. R. Chang and L.J. Graham: *J. Appl. Phys.*, 1966, vol. 37, pp. 3778-83.

36. P.B. Prangnell, T. Downes, W.M. Stobbs, and P.J. Withers: *Acta Metall. Mater.*, 1994, vol. 42, pp. 3425-36.
37. A.J. Allen, M.A.M. Bourke, S. Dawes, M.T. Hutchings, and P.J. Withers: *Acta Metall. Mater.*, 1992, vol. 40, pp. 2361-73.
38. C.A. Lewis, W.M. Stobbs, and P.J. Withers: *Mater. Sci. Eng.*, 1993, vol. A171, pp. 1-11.
39. T. Onda, Y. Bando, T. Ohba, and K. Otsuka: *Mater. Trans. JIM*, 1992, vol. 33, pp. 354-59.
40. K. Otsuka, T. Tamura, and K. Shimizu: *Phys. Status Solidi*, 1971, vol. 5, pp. 457-70.
41. S.P. Gupta and A.A. Johnson: *Trans. Jpn. Inst. Met.*, 1973, vol. 14, pp. 292-302.
42. O. Matsumoto, S. Myiazaki, K. Otsuka, and H. Tamura: *Acta Metall.*, 1987, vol. 35, pp. 2137-44.
43. B.A. Bilby and A.G. Crocker: *Proc. R. Soc. Lond.*, 1965, vol. 288A, pp. 240-55.
44. K.M. Knowles and D.A. Smith: *Acta Metall.*, 1981, vol. 29, pp. 101-10.
45. K. Mandagopal, J. Singh, and S. Banerjee: *Scripta Metall. Mater.*, 1991, vol. 25, pp. 2153-58.
46. M.F. Ashby: in *2nd Int. Conf. on the Strength of Metals and Alloys*, Pacific Grove, CA, ASM, Metals Park, OH, 1970, pp. 507-41.
47. M.F. Ashby: *Phil. Mag.*, 1970, vol. 21, pp. 399-424.
48. R.J. Wasilewski: in *Shape Memory Effects in Alloys*, J. Perkins ed., Plenum Publishing, NY, 1975, pp. 245-71.
49. J.F. Nye: *Physical Properties of Crystals*, Oxford University Press, Oxford, United Kingdom, 1985.
50. J.D. Eshelby: *Proc. R. Soc. Lond.*, 1957, vol. A241, p. 376.
51. P.J. Withers, W.M. Stobbs, and O.B. Pedersen: *Acta Metall.*, 1989, vol. 37, pp. 3061-84.
52. H.J. Frost and M.F. Ashby: *Deformation-Mechanism Maps: The Plasticity and Creep of Metals and Ceramics*, Pergamon Press, Elmsford, NY, 1982, p. 166.
53. *ASM Handbook: Alloy Phase Diagrams*, ASM, Materials Park, OH, 1992, p. 319.